A&A 471, 849–863 (2007)
DOI: 10.1051/0004-6361:20066608

Astronomy & Astrophysics

A survey of $[D_2CO]/[H_2CO]$ and $[N_2D^+]/[N_2H^+]$ ratios towards protostellar cores⋆

H. Roberts and T. J. Millar

School of Mathematics and Physics, Queens University Belfast, Belfast, BT7 1NN, UK
e-mail: helenroberts77@gmail.com

Received 20 October 2006 / Accepted 18 June 2007

ABSTRACT

Aims. We use observations and models of molecular D/H ratios to probe the physical conditions and chemical history of the gas and to differentiate between gas-phase and grain-surface chemical processing in star forming regions.
Methods. As a follow up to previous observations of $HDCO/H_2CO$ and DCN/HCN ratios in a selection of low-mass protostellar cores, we have measured D_2CO/H_2CO and N_2D^+/N_2H^+ ratios in these same sources. For comparison, we have also measured N_2D^+/N_2H^+ ratios towards several starless cores and have searched for N_2D^+ and deuterated formaldehyde towards hot molecular cores (HMCs) associated with high mass star formation. We compare our results with predictions from detailed chemical models, and to other observations made in these sources.
Results. Towards the starless cores and low-mass protostellar sources we have found very high N_2D^+ fractionation, which suggests that the bulk of the gas in these regions is cold and heavily depleted. The non-detections of N_2D^+ in the HMCs indicate higher temperatures. We did detect HDCO towards two of the HMCs, with abundances 1–3% of H_2CO. These are the first detections of deuterated formaldehyde in high mass sources since Turner (1990) measured $HDCO/H_2CO$ and D_2CO/H_2CO towards the Orion Compact Ridge.

Key words. ISM: molecules – ISM: clouds – ISM: abundances – stars: formation – astrochemistry

1. Introduction

Observations of deuterated molecules have become an important tool in the study of interstellar chemistry and star formation. Although the underlying (or cosmic) D/H ratio is low ($\sim 10^{-5}$), the formation of deuterated molecules is preferred at low temperatures ($\leq$80 K) and leads to a high degree of fractionation in dark molecular clouds ($T_{\rm kin} \sim 10$ K, $n(H_2) \gtrsim 10^4$ cm^{-3}). The level of fractionation is also affected by the abundance of neutral species (e.g. CO, N_2, CS) in the gas, which depends on the balance between accretion onto and evaporation from dust grains. Observations of cold, centrally condensed cores (some of which may be the the birthplace of future stars) show "holes" in the emission from typically abundant molecules such as CS and CO at the dust peak (e.g. Caselli et al. 1999; Bergin et al. 2001; Redman et al. 2002). This suggests that, at densities $\gtrsim 10^5$ cm^{-3}, for heavier species, accretion is "winning". Observations confirm that molecular D/H ratios do increase with increasing density and CO depletion (Caselli et al. 1999; Bacmann et al. 2002, 2003).

Enhanced molecular D/H ratios are also observed in the envelopes surrounding newly born stars where the gas is $\gtrsim$50 K and the material accreted onto the grains has evaporated. In fact, the highest levels of deuterium fractionation measured to date have been seen towards low-mass protostellar cores: $NH_2D/NH_3 > 0.1$ (Saito et al. 2000; Hatchell 2003), $ND_3/NH_3 = 0.001$ (van der Tak et al. 2002; Lis et al. 2002), $D_2CO/H_2CO = 0.05-0.4$ (Loinard et al. 2000, 2001; Ceccarelli et al. 2001), $CH_2DOH/CH_3OH = 0.3$, $CHD_2OH/CH_3OH = 0.06$, $CD_3OH/CH_3OH = 0.01$ (Parise et al. 2002, 2004), $D_2S/HDS = 0.1$ (Vastel et al. 2003). Note that molecules have been observed with 3 deuterium atoms substituted for hydrogen – based on the cosmic D/H ratio we would expect such isotopologues to be $\sim 10^{15}$ times less abundant, so the ND_3/NH_3 and CD_3OH/CH_3OH ratios represent enhancements of $\gtrsim 10^{12}$ orders of magnitude.

In "hot molecular cores" (HMCs) associated with high-mass star formation, which are clumps of dense gas with temperatures $\sim$100–200 K, the D/H ratios which have been measured are generally $\sim 10^{-3}$ (e.g. Hatchell et al. 1998a, 1999, and references therein), lower than the low-mass sources, yet still much higher than the cosmic value.

It is now generally accepted that the deuterium fractionation seen in warm gas was set during the colder prestellar core phase, when material was freezing onto grain surfaces. Once some heating event, such as the formation of the star or the passage of a shock, causes the grain mantles to evaporate the D/H ratios can survive for 10^4–10^6 yr in warm gas (Rodgers & Millar 1996; Osamura et al. 2004). Recent theoretical modelling by Doty et al. (2006) suggests that hot cores in both high and low mass protostellar sources will survive for only $\sim$a few $\times 10^3$–10^4 yr after the formation of the protostar. This means that chemistry in the gas-phase would not have time to significantly alter the composition of the gas post-evaporation. Thus, observing the warm gas around young protostars can provide valuable information about the physical conditions in the cold, accreting gas, before the onset of star formation. For example, the lower fractionation towards HMCs may suggest that the gas from which these stars formed was initially warmer, or that the low temperature accretion phase did not last long enough to produce very high fractionation.

⋆ Figures 1–5 are only available in electronic form at http://www.aanda.org

The composition of the gas surrounding a newly formed protostar is influenced by both gas-phase ion-molecule chemistry and reactions on the grain surfaces. Saturated species which do not form efficiently in the gas-phase at low temperatures (e.g. CH_3OH and H_2S) are readily observed, and the level of deuterium fractionation in these species (certainly for the low-mass sources, see above) indicates that the surface chemistry occurred during the cold, prestellar core phase. Recent observations of the envelopes surrounding low-mass protostars show jumps in abundance close to the protostar for several molecules, including H_2O, H_2CO, CH_3OH, SO and SO_2 (Ceccarelli et al. 2000a,b; Schöier et al. 2002; Maret et al. 2004, 2005). Maret et al. (2004), who surveyed H_2CO abundances, found the best fit to their data if the temperature is higher than 50 K within ∼100 AU of the protostar.

Roberts et al. (2002a, hereafter Paper I) surveyed a number of low-mass protostellar sources in DCN and HDCO, concluding that the fractionation was consistent with gas-phase chemistry and accretion over a period of $\lesssim$50 000 yr, but the chemical model used for comparison may have overestimated the formaldehyde fractionation (Osamura et al. 2005). By also obtaining D_2CO/H_2CO ratios, we can compare successive levels of deuteration (e.g. D_2CO/HDCO and HDCO/H_2CO) which will differ depending on whether the molecules have a gas-phase or grain-surface origin (Turner 1990; Rodgers & Charnley 2002).

Loinard et al. (2002) measured D_2CO/H_2CO ratios of 0.02−0.4 towards ∼20 low-mass protostellar sources, but did not detect D_2CO towards 6 more massive protostars ($D_2CO/H_2CO < 0.01$). Our survey of low-mass sources overlaps with theirs, but we also chose three different high-mass sources to survey. These are line-rich HMCs, drawn from those surveyed by Hatchell et al. (1998b), which show evidence of grain surface chemistry through large abundances of complex hydrogenated molecules and in which other molecular D/H ratios have been determined (Gensheimer et al. 1996; Hatchell et al. 1998a, 1999).

We have also surveyed N_2D^+ fractionation towards both the low and high mass protostellar cores in order to investigate the fractionation in the cold envelopes around the protostars. Molecular ions trace gas-phase chemistry: in dark clouds H_2 is ionised by cosmic rays and rapidly converted to H_3^+. Due to its low proton affinity, H_3^+ reacts with most other neutral species: e.g. CO and N_2, giving HCO^+ and N_2H^+. As N_2 appears to be less susceptible to freeze-out than CO, the N_2D^+/N_2H^+ ratio is a good tracer of deuteration in cold, dense, CO-depleted cores. Currently, it is unclear whether N_2H^+ remains in the gas-phase after CO freezes out due to a difference in the surface binding energies of N_2 and CO (Bergin & Langer 1997) or, as recent experimental work shows no evidence for this (Öberg et al. 2005), to differences in their formation and destruction rates in the gas-phase (Aikawa et al. 2001; Vastel et al. 2006). By comparing N_2D^+/N_2H^+ and DCO^+/HCO^+ ratios we should be able to eliminate many of the uncertainties in the underlying chemical network and see how the different distributions of N-bearing species in prestellar cores can be explained. We have also measured N_2D^+/N_2H^+ ratios towards a number of starless cores and we present these data for comparison. The sources are listed in Table 1.

Sections 2 and 3 describe the observations and data reduction techniques, presenting the resulting column densities and molecular D/H ratios. In Sect. 4 we discuss these results and in Sect. 5 present comparisons with theory and with chemical models.

2. Observations

The low-mass protostellar sources include those in which we have already determined HDCO/H_2CO and DCN/HCN ratios using the University of Arizona's (UofA) 12 m radio telescope, at Kitt Peak, Arizona (Paper I). The lines we observed are listed in Table 2, along with associated molecular data (determined using the JPL molecular spectroscopy catalogue[1] and the CDMS[2]) and telescope FWHM beamwidths.

Initially, we set out to observe the $4_{0,4}-3_{0,3}$ line of D_2CO at 231 GHz (Dec. 2001−Jan. 2002) with the James Clerk Maxwell Telescope (JCMT), on Mauna Kea, Hawaii, but the band in which the D_2CO line was observed also covered the 3−2 transition of N_2D^+. As N_2D^+ is believed to be a good tracer of gas-phase deuteration and depletion (see above) it was interesting that the N_2D^+ line was strong (∼1 K) in three of these sources, L1448NW, L1448mms and HH211, but absent (at a level of <0.1 K) in L1527 and L1551 IRS5. We wished to determine whether this apparent difference in abundance also corresponded to a difference in deuterium fractionation.

In December 2002 we observed the ground state transitions of N_2H^+ and N_2D^+ and selected 2−1 lines of $H_2^{13}CO$, HDCO and D_2CO (see Table 2) towards high and low mass star forming regions with the UofA 12 m telescope. The N_2D^+ and N_2H^+ $J = 1-0$ lines towards the starless cores were observed in June 2002.

We used the IRAM 30 m telescope at Pico Veleta, Spain, in February 2005, primarily to observe the 3−2 transition of N_2H^+, but we were also able to simultaneously re-observe the N_2D^+ 3−2 line. Finally, in June 2005 we made further JCMT observations of the N_2D^+ 3−2 multiplet and D_2CO $4_{0,4}-3_{0,3}$ lines towards 6 additional low-mass protostellar sources.

The spectra are shown in Figs. 1–5[3]. Spectra towards the starless cores are shown in Fig. 1, the spectra for the low-mass protostellar sources are shown in Figs. 2−4, while those observed towards the HMCs are shown in Fig. 5. In all cases, the observations are shaded grey, while the fits are shown as solid black lines. All spectra have beam scaled to the main-beam temperature scale, and the source velocity (see Table 1) has been subtracted from the velocity scale.

2.1. UofA 12 m telescope data

The 3 mm receivers were used to observe the N_2H^+ and N_2D^+ ground-state transitions and the D_2CO $2_{1,2}-1_{1,1}$ transition, while the 2 mm receiver was used for the HDCO and $H_2^{13}CO$ lines. The observations were carried out in position-switching mode, using beam throws of 10−30′ in azimuth (the off-positions were first checked for excess emission). The Millimeter AutoCorrelator (MAC) correlation spectrometer was used with 49 kHz resolution ($\lesssim$0.2 km s^{-1}). In December 2002, typical system temperatures were 150−300 K. In June 2002 the system temperatures were 350−450 K for the N_2D^+ lines and 200−250 K for the N_2H^+ lines. Pointing was checked every two hours or so and errors found to be $\lesssim$5−6″. The data were calibrated by the usual chopper wheel method and then corrected for η_m^*, the efficiency at which the source couples to the main diffraction beam, to give $T_{\rm MB}$.

The N_2H^+ 1–0 multiplet was detected towards all the starless cores, while the N_2D^+ 1–0 multiplet was seen in only three out of

[1] Jet Propulsion Laboratory: http://spec.jpl.nasa.gov/

[2] Cologne Database for Molecular Spectroscopy: http://www.ph1.uni-koeln.de/vorhersagen/

[3] Online version only.

Table 1. Sources observed, along with velocities, bolometric temperatures and protostellar classes (where applicable) taken from the literature.

Region	Source	α_{2000} [h m s]	δ_{2000} [° ′ ″]	v_{lsr} (km s^{-1})	T_{bol} (K)	Class
Low-mass protostellar cores						
Perseus	L1448 mms	03:25:38.8	+30:44:05.3	+5.6	60	0
″	L1448 NW	03:25:35.6	+30:45:34.2	+5.0	55	0
″	HH211	03:43:56.8	+32:00:50.2	+9.2	30	0
″	NGC 1333 IRAS 4A	03:26:04.8	+31.03.14.0	+7.0	34	0
″	B1	03:33:20.8	+31:07:34.1	+6.5	–	0
″	B5 IRS1	03:47:41.3	+32:51:42.0	+10.2	85	I
″	IRAS 03282	03:31:20.4	+30:45:25.0	+7.0	26	0
Taurus	L1527	04:39:53.5	+26:03:05.5	+5.6	59	0
″	L1551 IRS5	04:31:34.1	+18:08:05.0	+6.4	97	I
Orion	RNO43	05:32:19.4	+12:49:32.0	+9.6	33	0
″	HH111	05:51:46.3	+02:48:30.0	+8.5	38	0
Serpens	S68N	18:29:48.2	+01:16:53.5	−2.0	–	0
Other	L1157	20:39:06.5	+68:02:13.4	+2.0	62	0
Hot molecular cores						
	G31.41	18:47:34.2	−01:12:46.0	+97.4		
	G34.26	18:53:18.6	+01:14:58.2	+58.0		
	G75.78	20:21:44.1	+37:26:39.7	−0.1		
Starless cores						
	L1517B	05:00:19.0	+30:37:42.8	+5.7		
	L1400G	04:25:05.6	+54:58:53.2	+3.4		
	L1498	04:10:51.5	+25:09:58.3	+7.7		
	TMC-2	04:32:44.8	+24:25:12.5	+6.2		
	L1512	05:04:09.5	+32:43:08.6	+7.1		

Table 2. Molecular line data.

Transition	ν_{ul} (GHz)	E_u (K)	A_{ul} (s^{-1})	Telescope	Beamsize (″)
N_2D^+ 1–0	77.1093	3.7	2.056×10^{-5}	UofA 12 m	80
N_2H^+ 1–0	93.1734	4.47	3.38×10^{-5}	UofA 12 m	70
para-D_2CO $2_{1,2}$–$1_{1,1}$	110.8378	13.4	2.58×10^{-5}	UofA 12 m	58
HDCO $2_{1,1}$–$1_{1,0}$	134.2848	17.6	4.59×10^{-5}	UofA 12 m	50
ortho-$H_2^{13}CO$ $2_{1,2}$–$1_{1,1}$	137.450	21.7	4.93×10^{-5}	UofA 12 m	50
N_2D^+ 3–2	231.3219	22.2	7.14×10^{-4}	JCMT/IRAM	21/10
ortho-D_2CO $4_{0,4}$–$3_{0,3}$	231.4102	27.9	3.47×10^{-4}	JCMT	21
N_2H^+ 3–2	279.5117	26.8	1.26×10^{-3}	IRAM	9

the five (Fig. 1). For the five low-mass protostellar cores which we set out to observe, the N_2H^+, N_2D^+ and the D_2CO $2_{1,2}$–$1_{1,1}$ line were seen towards all sources (Fig. 2). We also tried to increase the sample of low-mass protostellar sources from those in Paper I, but did not obtain a full set of data; the spectra observed towards these extra sources are shown in Fig. 4. $H_2^{13}CO$ and N_2H^+ were detected towards all three of the HMCs, HDCO was detected in only two of them, and N_2D^+ was not detected at all in the high-mass sources (Fig. 5).

2.2. JCMT data

The JCMT observations of the low-mass sources were carried out in beam-switching mode, using a chop-throw of −180″ in azimuth. The HMCs were observed in position-switching mode using off-positions from Hatchell et al. (1999). The Digital Autocorrelation Spectrometer (DAS) was used with a bandwidth of 760 MHz, giving a spectral resolution of ∼0.2 km s^{-1}. The data were corrected for $\eta_{fss}\eta_{mb}$ (the "forward scattering and spillover" and "main beam" efficiencies) to put the spectra on the main beam scale. This assumes that the source is extended, relative to the beam, which we believe to be the case for the low-mass protostellar envelopes (see later). In total, nine low-mass protostellar sources were observed (Figs. 2 and 3). The D_2CO $4_{0,4}$–$3_{0,3}$ line was detected towards all but two (B5IRS1 and HH111) of these, while the N_2D^+ 3−2 multiplet was weak or absent towards L1527, L1551IRS5, B5IRS1, HH111 and RNO43, but strong towards the other sources.

2.3. IRAM data

The observations were carried out in position switching mode, with an offset 20′E. Due to bad weather (snow) we were only able to observe three sources and the spectra we did obtain have rather bad baselines (see Fig. 2). These spectra have a resolution of 0.1 km s^{-1} and a correction factor of F_{eff}/B_{eff} (the ratio of the forward efficiency to the main beam efficiency) was used to convert to the main beam scale. Again, this assumes the sources are extended relative to the beam.

3. Data reduction

In all cases we have assumed a filling factor of 1; the implications of this are discussed later, when we compare our results to other observations. As we are primarily interested in the ratios

Table 3. Noise levels and integrated intensities for the formaldehyde lines, along with upper-level column densities calculated assuming optically thin lines.

Source	rms (K)	$\int T_{MB} dv$ (K km s^{-1})	N_u (10^{10} cm^{-2})
$H_2^{13}CO$ $2_{1,2}$–$1_{1,1}$			
L1157	0.02	0.106 (±0.007)	7.91 (±0.54)
G31.41	0.02	0.524 (±0.023)	39.0 (±1.69)
G34.26	0.03	1.335 (±0.027)	99.4 (±2.05)
G75.78	0.04	0.296 (±0.025)	22.0 (±1.89)
HDCO $2_{1,1}$–$1_{1,0}$			
L1157	0.02	0.101 (±0.010)	7.70 (±0.80)
NGC 1333 4A	0.03	0.481 (±0.014)	36.7 (±1.06)
G31.41	0.01	–	<2.75
G34.26	0.02	0.415 (±0.016)	31.7 (±1.20)
G75.78	0.01	0.273 (±0.010)	20.9 (±0.77)
D_2CO $2_{1,2}$–$1_{1,1}$			
L1448NW	0.02	0.073 (±0.009)	6.71 (±0.85)
L1448mms	0.01	0.052 (±0.005)	4.83 (±0.48)
HH211	0.01	0.051 (±0.004)	4.75 (±0.40)
L1527	0.01	0.035 (±0.004)	3.23 (±0.37)
L1551IRS5	0.02	0.078 (±0.008)	7.19 (±0.76)
NGC 1333 4A	0.02	0.182 (±0.009)	16.8 (±0.86)
G34.26	0.01	–	<1.85
G75.78	0.01	–	<3.28
D_2CO $4_{0,4}$–$3_{0,3}$			
L1448NW	0.04	0.375 (±0.031)	11.2 (±0.91)
L1448mms	0.04	0.253 (±0.021)	7.58 (±0.63)
HH211	0.07	0.244 (±0.042)	7.30 (±1.24)
L1527	0.04	0.180 (±0.019)	5.38 (±0.56)
L1551IRS5	0.09	0.217 (±0.042)	6.50 (±1.24)
NGC 1333 4A	0.08	0.182 (±0.051)	5.47 (±1.52)
B1	0.06	0.275 (±0.034)	8.24 (±1.01)
B5IRS1	0.06	–	<3.22
RNO43	0.06	0.222 (±0.040)	6.65 (±1.21)
HH111	0.10	–	<4.89
IRAS03282	0.07	0.090 (±0.032)	2.70 (±0.97)

of our column densities, however, any errors introduced by this assumption should cancel out.

3.1. Formaldehyde

Gaussians fits to the detected lines are shown in Figs. 2–5. Based on our previous observations of different isotopomers of formaldehyde in these sources (Paper I) we expect that the $H_2^{13}CO$, HDCO and D_2CO lines will be optically thin. We can, therefore, calculate the column density of molecules in the upper level of the transition (N_u) from the integrated intensities of the lines using the standard formula:

$$\int T_{MB} dv = \frac{A_{ul} h c^3}{8\pi k \nu^2} N_u \quad (1)$$

(cf. Goldsmith & Langer 1999, where we use T_{MB} rather than T_a as appropriate for extended sources and for consistency between the different telescopes).

The parameters of the Gaussian fits and the resulting upper level column densities are listed in Table 3. In the event that a line was not detected, we have calculated 3σ upper limits on the column density using the linewidths that we measured for other formaldehyde lines in the same source.

In order to calculate total column densities we need some estimate of the excitation (rotation) temperature, T_{ex}. We assume local thermodynamic equilibrium (LTE) holds, then:

$$N_u = \frac{g_u}{Q(T_{ex})} \exp(-E_u/kT_{ex}) N_{TOT}. \quad (2)$$

The ortho and para forms of D_2CO can be treated as separate species, with different partition functions, $Q(T_{ex})$. These have been calculated at different excitation temperatures using energy-level data in the JPL catalogue.

The high-temperature statistical o/p ratio for D_2CO is 2, but it is unclear what the actual value will be for interstellar molecules. For H_2CO, Dickens & Irvine (1999) found o/p ratios between 1.5 and 2 towards star-forming cores with outflows, rather than the high-temperature statistical value of 3, indicating that the formaldehyde formed at low temperatures (10–20 K; Kahane et al. 1984).

There are six source in which we observed both ortho- and para-D_2CO. Calculating N_{tot} with $T_{ex} \sim 18$ K (7 and 11 K for NGC 1333 4A and L1551IRS5, respectively) results in column densities of o-D_2CO being twice as high as p-D_2CO (o/p ~ 2:1). An o/p ratio of 3:1 results from using excitation temperatures ~2–6 K different, but the total $N(D_2CO)$ values are changed by <10%. We have recalculated the HDCO and H_2CO column densities from Paper I using consistent T_{ex} values; these are listed in Table 4. The uncertainty in the o/p ratio and T_{ex} gives overall uncertainties of ~30% for $N(H_2^{13}CO)$. The $^{12}C/^{13}C$ ratio is not particularly well determined in molecular clouds: we have adopted a value of 60, but 75 might be more appropriate. This is an uncertainty of ~25%, but it is smaller than the overall uncertainties quoted in Table 4, and, of course, varying the $^{12}C/^{13}C$ ratio would change the HDCO/H_2CO and D_2CO/H_2CO ratios by the same amount.

Those sources where we give a range of values for $N(H_2CO)$ and the resulting fractionation are those in which we did not detect $H_2^{13}CO$ and so were unable to determine the optical depth of the main H_2CO line. For the other sources, the overall uncertainties in the D/H ratios resulting from the uncertainty in T_{ex} and the o/p ratio are ~30%, similar to the uncertainty arising from the noise in the spectra. We, therefore, quote HDCO/H_2CO and D_2CO/H_2CO ratios with errors of 40–50%.

For the HMCs, where we believe that the bulk of the gas is warmer (Hatchell et al. 1998a,b) we have adopted a value of $T_{ex} = 50$ K. Increasing the excitation temperature from 50 to 150 K does increase the column density estimates by factors of 3–5, but reduces the calculated HDCO/H_2CO ratios by less than a factor of 2 and has little effect on the D_2CO/H_2CO limits.

For the low-mass sources, the range of HDCO fractionation is ~0.02–0.07, while the D_2CO fractionation is ~0.01–0.04. In those sources where we have good $N(H_2CO)$ determinations, L1551 IRS5 has the highest fractionation, while HH211 has the lowest. There is a larger variation towards the HMCs, with the HDCO/H_2CO ratio in G31.41 being more than an order of magnitude lower than in G75.78.

We note that the D_2CO $2_{1,2}$–$1_{1,1}$ and $4_{0,4}$–$3_{0,3}$ lines were observed with different telescopes, whose beamwidths differ by a factor ~3. Without knowing the spatial distribution of the formaldehyde emission around the source it is difficult to correct for this. If we assume that the region containing formaldehyde is roughly less than the area of the JCMT beam (the smaller beam) then we are underestimating the column density of D_2CO molecules in the the $J = 2_{1,2}$ level (which was observed with the larger beam). For the sources where we observed the D_2CO 2–1 line with the UofA 12 m telescope,

Table 4. Excitation temperatures, formaldehyde column densities and molecular D/H ratios. $N(H_2CO)$ and $N(HDCO)$ come from Paper I, except for L1157 and NGC 1333 IRAS 4A where they come from the 2−1 line data in Table 3.

Source	T_{ex} (K)	$N(D_2CO)$ (10^{11} cm^{-2})	$N(HDCO)$ (10^{12} cm^{-2})	$N(H_2CO)$ (10^{13} cm^{-2})	HDCO/H_2CO	D_2CO/H_2CO	F (see text)
L1448NW	18	16.56 (±1.50)	4.64 (±0.79)	7.47 (±2.78)	0.06 (±0.025)	0.02 (0.008)	0.2
L1448mms	18	11.44 (±1.00)	1.45 (±0.88)	1.46–4.29	0.03–0.1	0.03–0.08	0.03–0.1
HH211	18	11.09 (±1.50)	1.71 (±0.24)	7.80 (±3.33)	0.02 (±0.01)	0.01 (0.006)	0.04
L1527	18	7.96 (±1.00)	2.72 (±0.30)	4.56 (±1.23)	0.06 (±0.025)	0.02 (0.008)	0.2
L1551IRS5	11	13.07 (±2.00)	2.09 (±0.36)	3.07 (±0.61)	0.07 (±0.03)	0.04 (0.016)	0.1
NGC 1333 4A	7	27.38 (±5.00)	5.81 (±0.17)	–	0.034[a]	0.02[a]	0.06
B1	18	12.36 (±1.50)	–	–	–	–	
B5IRS1	18	<4.83	0.62 (±0.39)	0.56–3.51	0.02–0.11	<0.09	–
RNO43	18	9.97 (±1.80)	<1.24	0.63–3.70	0.03–0.2	0.03–0.16	0.03–0.25
HH111	18	<7.33	1.26 (±0.59)	4.39 (±2.17)	0.03 (±0.01)	<0.02	>0.04
IRAS03282	18	4.05 (±1.50)	0.84 (±0.34)	0.67–4.26	0.02–0.12	0.01–0.06	0.04–0.24
L1157	18	–	1.16 (±0.12)	4.91 (±0.34)	0.02 (±0.01)	–	–
G31.41	50	–	<1.03	47.16 (±2.04)	<0.002	–	–
G34.26	50	<15.96	11.91 (±0.45)	120.2 (±2.48)	0.01 (±0.001)	<0.001	>0.1
G75.78	50	<28.30	7.85 (±0.29)	26.60 (±2.29)	0.03 (±0.003)	<0.01	>0.1

Notes: We assumed a $^{12}C/^{13}C$ ratio of 60; the ortho/para ratio is ∼2:1 (see text). [a]Using the H_2CO column density of 1.7×10^{14} cm^{-2} calculated by Maret et al. (2004), see Table 7.

applying beam filling factors will have little effect on our estimated D_2CO/H_2CO ratios, since both the H_2CO and D_2CO column densities will be similarly affected. For the sources in which we have only observed one D_2CO line (the $4_{0,4}-3_{0,3}$ line using the JCMT), applying a beam correction factor will lower the D_2CO/H_2CO ratios, since assuming a small source size will increase the H_2CO column density determinations from the UofA 12 m data. The D_2CO/H_2CO ratios towards B5IRS1, RNO43, HH111 and IRAS03282 would then be $\lesssim$0.001.

While Maret et al. (2004) did find evidence for jumps in H_2CO abundance very close to the protostar, significant amounts of formaldehyde were also present in the larger envelope. Also, when Ceccarelli et al. (2001) mapped the D_2CO emission around the low-mass protostar IRAS 16293-2422 they found that it extends 40″ south of the protostar, so the D_2CO emission in the cores we have observed could be extended enough to fill even the 60″ beam of the UofA 12 m telescope.

3.2. Diazenylium

The 1–0 and 3–2 transitions of N_2H^+ and N_2D^+ have hyperfine structure, which we can use to get an estimate of the optical depths. We took the positions and relative intensities of the hfs components from Womack et al. (1992), Dore et al. (2004), Caselli et al. (2002a), and Gerin et al. (2001) for N_2H^+ $J = 1-0$, N_2D^+ $J = 1-0$, N_2H^+ $J = 3-2$ and N_2D^+ $J = 3-2$, respectively, and used the "HFS" method of the data reduction program CLASS[4] to fit the spectra. These fits are shown in Figs. 1−5 and the fit parameters are listed in Table 5. In most cases the transitions were optically thin, or had only moderate optical depth. This was corrected for, where necessary, in the calculation of the upper level column densities listed in Table 5.

Unfortunately, a lot of the IRAM data had bad baselines – almost sinusoidal (see Fig. 2, row 4) – which may be confusing the CLASS fitting algorithm when it looks for outlying HFS components. Comparing the JCMT and IRAM data for L1448mms and L1448NW, the height of the main lines are fairly consistent when all sets of data are converted to the T_{mb} scale, but the overall line shapes and CLASS fits differ significantly. The column densities based on the fits to the IRAM data have, therefore, been calculated assuming $\tau = 0.1$ and are strictly lower limits.

Fits to the N_2D^+ 3–2 multiplet observed at the JCMT show significant optical depth towards L1448NW and L1448mms. For HH211, the fit parameters had high uncertainties and so we have forced an optically thin fit which, again, gives only a lower limit on the column density.

For diazenylium, the uncertainty in the excitation temperature swamps the other observational uncertainties. In Table 6 we have adopted $T_{ex} = 12$ K for the cold cores and other low-mass sources and 50 K for the HMCs. We note that varying T_{ex} between 5 and 30 K changes the column density determinations by less than a factor of a three and changes the D/H ratio determinations by <20%. We have, therefore, listed the N_2D^+/N_2H^+ in Table 6 with an overall error of ±15%. Varying the excitation temperature in the HMCs from 50 to 150 K has a negligible effect on the tabulated upper limits.

4. Discussion of results

Three of the cold cores and four of the low-mass protostellar sources have very high N_2D^+/N_2H^+ ratios: 0.16−0.3. These are comparable to the values seen towards the prestellar cores L134N (Gerin et al. 2001) and L1544 (Caselli et al. 2002b). The other two low-mass sources have ratios of 0.06 and 0.08, while the fractionation in the other two cold cores (L1517B and L1498) is <0.02. We note that Gerin et al. (2001) determined N_2D^+/N_2H^+ to be 0.15 towards B1, which is slightly lower than the value of 0.25 we obtained (though the two values agree to within stated uncertainties), and that Crapsi et al. (2005) did detect N_2D^+ towards L1498 with $N_2D^+/N_2H^+ \sim 0.04$. Both these studies used the IRAM 30 m telescope whereas L1498 was observed by us only with the ARO 12 m telescope, so the latter discrepancy is explained by beam dilution.

L1527 and L1551 IRS5, the low-mass protostellar sources with the lowest N_2D^+/N_2H^+ ratios, are the only two sources in our survey from the Taurus molecular cloud. Measurements of other molecular D/H ratios though, (e.g. HDCO, D_2CO, DCN) do not show systematic differences between clouds. Hatchell (2003) did measure NH_2D/NH_3 ratios towards these

[4] Part of the GILDAS data reduction package: `http://www.iram.fr/IRAMFR/GILDAS`

Table 5. CLASS fits to the multiplet transitions of N_2D^+ and N_2H^+ and resulting upper level column densities.

Source	v_{lsr} (km s^{-1})	Δv (km s^{-1})	τ^1	$\int T_{MB}\,\Delta v$ (K km s^{-1})	rms (K)	N_u (10^{11} cm^{-2})
N_2H^+ 1–0 (UofA 12 m)						
L1512	6.59	0.35	0.28	1.550	0.05	7.75 (±0.07)
L1517B	5.30	0.39	0.20	1.320	0.05	6.60 (±0.08)
L1400G	2.96	0.49	0.20	1.264	0.04	6.32 (±0.06)
L1498	7.31	0.42	0.13	1.824	0.07	9.11 (±0.11)
TMC-2	5.70	0.45	0.15	2.577	0.06	12.9 (±0.09)
L1448NW	4.95	1.03	0.16	13.55	0.03	67.7 (±0.06)
L1448mms	5.43	1.14	0.10	7.686	0.02	38.4 (±0.06)
HH211	9.49	0.73	0.10	3.422	0.03	17.1 (±0.05)
L1527	6.38	0.50	0.17	2.665	0.03	13.3 (±0.05)
L1551	6.91	0.82	0.10	7.709	0.02	38.5 (±0.04)
B1	6.08	0.93	0.19	9.626	0.05	48.1 (±0.11)
G31.41	97.36	4.06	0.10	11.55	0.04	57.7 (±0.19)
G34.26	58.83	3.61	0.10	42.68	0.04	213 (±0.15)
G75.78	0.63	3.00	0.10	9.346	0.03	46.7 (±0.13)
N_2D^+ 1–0 (UofA 12 m)						
L1512	7.25	0.41	0.10	0.207	0.04	1.16 (±0.05)
L1517B	–	0.39	–	–	0.03	<0.13
L1400G	3.44	0.42	0.10	0.191	0.03	1.07 (±0.04)
L1498	–	0.42	–	–	0.02	<0.11
TMC-2	6.30	0.50	0.10	0.336	0.03	1.89 (±0.05)
L1448NW	4.45	0.85	0.14	2.355	0.04	13.2 (±0.08)
L1448mms	4.94	1.40	0.10	1.021	0.03	5.74 (±0.07)
HH211	9.08	0.82	0.10	0.841	0.02	4.73 (±0.05)
L1527	6.01	0.65	0.14	0.119	0.01	0.67 (±0.02)
L1551	6.50	0.80	0.10	0.502	0.02	2.82 (±0.04)
L1157	2.72	0.50	0.10	0.274	0.02	1.54 (±0.03)
NGC 1333 IRAS 4A	7.58	1.23	0.10	1.879	0.04	10.6 (±0.10)
B1	6.73	0.89	0.10	1.873	0.07	10.5 (±0.15)
S68N	8.68	1.05	0.55	0.675	0.02	3.79 (±0.06)
G34.26	–	3.60	–	–	0.01	<0.28
G75.78	–	3.00	–	–	0.02	<0.22
N_2H^+ 3–2 (IRAM)						
L1448NW	3.9	1.2	0.10	5.96	0.17	>7.49
L1448mms	5.1	1.0	0.10	8.93	0.24	>11.2
L1527	5.6	1.1	0.10	1.69	0.15	>2.13
N_2D^+ 3–2 (IRAM)						
L1448NW	4.3	1.2	0.10	3.906	0.09	>5.93
L1448mms	5.0	0.8	0.10	1.785	0.07	>2.71
N_2D^+ 3–2 (JCMT)						
L1448mms	119.98	0.59	2.32	4.623	0.04	6.73 (±0.03)
L1448NW	119.17	0.73	2.67	8.670	0.04	12.6 (±0.04)
L1527	–	0.60	–	–	0.04	<0.11
HH211	123.93	0.69	0.10	1.827	0.07	>2.66
L1551	–	0.80	–	–	0.09	<0.29
N_2D^+ 3–2 (JCMT June 2005)						
NGC 1333 IRAS 4A	–0.1	1.05	1.29	2.68	0.08	6.95 (±0.13)
B1	0.3	0.77	2.95	2.43	0.06	11.1 (±0.07)
B5IRS1	0.7	1.14	0.10	0.34	0.06	0.52 (±0.11)
RNO43	1.1	1.00	0.10	0.30	0.06	0.46 (±0.10)
HH111	0.3	1.29	0.10	0.26	0.10	0.39 (±0.19)
IRAS03282	0.3	0.81	0.47	1.05	0.07	1.92 (±0.08)

Note: [1]τ represents the overall optical depth (i.e. that of a hypothetical unsplit line).

same sources in Taurus to be more than a factor of 2 lower than those in Perseus and Orion, but concluded that the NH_2D column densities were being underestimated because of beam dilution.

L1551 IRS5 is a Class I source and has the highest bolometric temperature of the sources we observed, so the lower N_2D^+ fractionation could be due to its more evolved nature. L1527 has the narrowest line-widths of the protostellar sources, though, which indicates that its envelope is relatively undisturbed by the protostar. Interestingly, HH211, one of the least evolved Class 0 sources (by the, admittedly, crude measure of T_{bol}) has the highest N_2D^+/N_2H^+ ratio observed in this survey, while also having one of the lowest formaldehyde fractionation of the sources surveyed (see Table 4). Overall, though, the N_2D^+/N_2H^+ and D_2CO/H_2CO ratios show no sign of a correlation with T_{bol}.

Table 6. Column densities for N_2D^+ and N_2H^+, calculated using the excitation temperatures shown (see text), along with resulting N_2D^+/N_2H^+ ratios.

Source	$N_{tot}(N_2D^+)$ ($\times 10^{12}$ cm^{-2})	$N_{tot}(N_2H^+)$ ($\times 10^{12}$ cm^{-2})	N_2D^+/N_2H^+
L1512	0.36 (±0.03)	2.14 (±0.02)	0.17 (±0.02)
L1517B	<0.04	1.83 (±0.02)	<0.02
L1400G	0.33 (±0.02)	1.75 (±0.02)	0.19 (±0.03)
L1498	<0.03	2.52 (±0.03)	<0.01
TMC2	0.59 (±0.03)	3.57 (±0.03)	0.16 (±0.02)
L1448NW	4.09 (±0.06)	18.7 (±0.02)	0.22 (±0.03)
L1448mms	1.78 (±0.07)	10.6 (±0.02)	0.17 (±0.03)
HH211	1.46 (±0.04)	4.73 (±0.01)	0.31 (±0.05)
L1527	0.21 (±0.01)	3.68 (±0.01)	0.06 (±0.01)
L1551IRS5	0.87 (±0.03)	10.65 (±0.01)	0.08 (±0.01)
L1157	0.48 (±0.02)	–	–
NGC 1333 4A	3.29 (±0.08)	–	–
	3.25 (±0.11)	13.3 (±0.03)	0.25 (±0.04)
S68N	1.18 (±0.04)	–	
B5IRS1	0.32 (±0.07)	–	–
RNO43	0.29 (±0.06)	–	–
HH111	0.24 (±0.12)	–	–
IRAS03282	1.19 (±0.05)	–	–
G31.41	–	47.74 (±0.157)	–
G34.26	<0.275	176.2 (±0.124)	<0.002
G75.78	<0.216	38.64 (±0.108)	<0.006

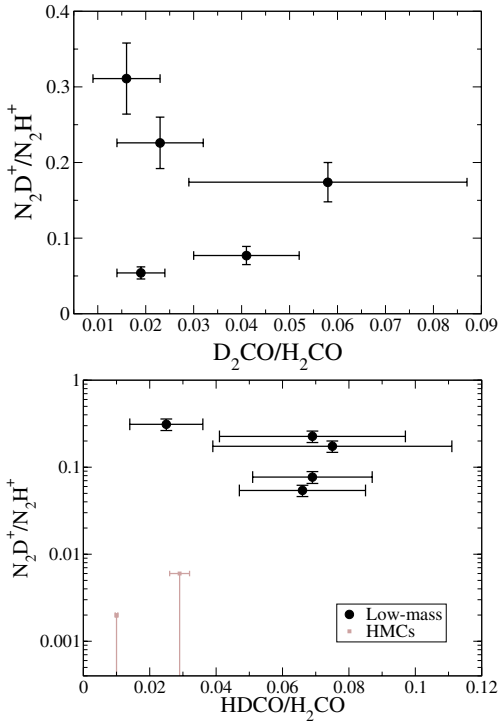

Fig. 6. *Top*: a comparison of the D_2CO/H_2CO and N_2D^+/N_2H^+ ratios observed towards the low-mass protostellar sources. *Bottom*: a comparison of the $HDCO/H_2CO$ and N_2D^+/N_2H^+ ratios observed towards the low-mass protostellar sources and HMCs.

In Fig. 6 we compare the N_2D^+/N_2H^+ ratios to both the D_2CO/H_2CO and $HDCO/H_2CO$ ratios to see if the formaldehyde and diazenylium fractionation are, in fact, anti-correlated. Unfortunately, we do not have data in enough sources to make a convincing case. For four of the sources it does seem that the N_2D^+/N_2H^+ ratios decrease as the D_2CO/H_2CO ratios increase, but results for L1527 are anomalous, as both the N_2D^+ and D_2CO fractionation are relatively low. Comparing the HDCO and N_2D^+ fractionation, the $HDCO/H_2CO$ ratios are very similar in most sources (∼0.06), while the N_2D^+ fractionation ranges from 0.06 to 0.2. Only HH211, which has the highest N_2D^+/N_2H^+ ratio measured in this survey and a $HDCO/H_2CO$ ratio of only 0.02, suggests an anti-correlation.

We have considered various line width comparisons:

- the D_2CO and N_2D^+ lines which were observed simultaneously with the JCMT have equal linewidths to within 25% (except L1448NW, where the D_2CO line was 1.5 times broader than the N_2D^+ line);
- the linewidths of the N_2H^+ and N_2D^+ 1−0 transitions in each source are similar, indicating that these molecules are indeed located in the same region of each source;
- as we expect, the cold cores generally have narrower lines that the protostellar sources, since the protostar disrupts its surrounding envelope increasing turbulence;
- we, therefore, compared the N_2D^+ fractionation to the N_2H^+ linewidth but found no evidence for an evolutionary trend.

4.1. A comparison with previous formaldehyde surveys

Using the IRAM 30 m telescope, Loinard et al. (2002) carried out a survey of D_2CO/H_2CO ratios towards protostellar sources, while, more recently, Parise et al. (2006) have determined methanol and formaldehyde fractionation towards a sample of low-mass protostellar cores (using data from Maret et al. 2004, 2005).

For the sources where our survey overlaps with that of Loinard et al. (2002), we calculate higher H_2CO column densities but similar D_2CO column densities and, thus, lower D_2CO/H_2CO ratios. Loinard et al. only observed the main isotopomer of H_2CO, though, and assumed that the transitions were optically thin, noting that this may underestimate the H_2CO column densities. The fact that our D_2CO column densities based on UofA 12 m data are not systematically lower than those from Loinard et al. using the IRAM 30 m telescope supports our assumption that the D_2CO emission is extended enough to fill the 60″ beam of the 12 m telescope.

For the three sources where our survey overlaps with that of Maret et al. (2004) and Parise et al. (2006), the H_2CO column densities we have determined are consistent with theirs (see Table 7). For D_2CO, however, their column densities (averaged over a 10″ beam) are ∼5−20 times higher than ours. This leads to their D_2CO/H_2CO ratios also being significantly higher. The D_2CO rotational temperatures from Parise et al. (2006) are only 5−6 K, but these are based on assuming a source size of 10″. The beamsizes we used for the D_2CO observations were 20 and 60″. As discussed above, including a beam dilution factor would increase our H_2CO column density estimates more than the D_2CO column densities, giving even worse agreement for the fractionation.

It is possible that the abundance and fractionation of deuterated formaldehyde increases closer to the protostar, but more gradually and over a larger radius than the sharp jump in H_2CO abundance which occurs when $T_{kin} > 50$ K and the ice mantles evaporate (within ∼100 AU of the protostar; Maret et al. 2004). Parise et al. (2006) note that the linewidths of the deuterated formaldehyde transitions they observed are narrower than those of the main isotopomer, suggesting that the HDCO and D_2CO emission is dominated by the cold, outer envelopes of the protostars. If D_2CO is extended then Parise et al. could have

Table 7. A comparison of our results with those from Maret et al. (2004) and Parise et al. (2006), using the IRAM 30 m telescope.

	N(H_2CO) (10^{13} cm^{-2})		$N(D_2CO)$ (10^{12} cm^{-2})		D_2CO/H_2CO	
	(Maret et al.)	(This work)	(Parise et al.)	(This work)	(Parise et al.)	(This work)
L1448NW[a]	11	8 ± 3	8.2	1.5 ± 0.2	0.08	0.02 ± 0.01
L1448mms[b]	4.2	3 ± 1.5	9.1	1 ± 0.1	0.24	0.05 ± 0.025
L1527	4.2	5 ± 1	15.	0.7 ± 0.1	0.44	0.016 ± 0.005
NGC 1333 IRAS 4A	17	–	19.	4 ± 2	0.12	0.02

[a]Also known as L1448-N; [b]also known as L1448-MM or L1448-C.

overestimated its column density by correcting for a 10″ source. Alternately, if the H_2CO is more extended than the D_2CO, then we may be underestimating the D_2CO fractionation in the inner regions. Thus, (as Parise et al. also noted), further observations to map the formaldehyde emission at a higher angular resolution are required.

5. Theory and chemical modelling

Diazenylium forms via proton transfer from H_3^+ and its deuterated analogues to N_2. The N_2D^+/N_2H^+ ratio, therefore, depends on the fractionation of deuterated H_3^+. H_3^+ is converted to its deuterated analogues via successive exchange reactions with HD (the interstellar reservoir of deuterium), a process which occurs more efficiently when other molecules that destroy H_3^+ (CO, O, N_2, etc.) are depleted onto grains. At temperatures $\gtrsim$25 K, deuterated H_3^+ is destroyed by reaction with H_2, reducing the fractionation of these and related molecules such as DCO^+ and N_2D^+. The N_2D^+/N_2H^+ ratios of >0.1 we have measured towards several sources suggests, therefore, that the bulk of the gas is cold and heavily depleted in CO.

In the gas-phase, formaldehyde primarily forms via the reaction chain:

$$CH_3^+ \xrightarrow{H_2} CH_5^+ \xrightarrow{e^-} CH_3 \xrightarrow{O} H_2CO, \quad (3)$$

which has deuterated analogues:

$$CH_2D^+ \xrightarrow{H_2} CH_4D^+ \xrightarrow{e^-} CH_2D \xrightarrow{O} HDCO \quad (4)$$

$$CHD_2^+ \xrightarrow{H_2} CH_3D_2^+ \xrightarrow{e^-} CHD_2 \xrightarrow{O} D_2CO. \quad (5)$$

The formaldehyde fractionation, therefore, depends on the fractionation of deuterated CH_3^+. Like H_3^+, CH_3^+ is a "primary ion" for deuterium fractionation since it is also converted to its deuterated analogues via successive reactions with HD and the reverse reactions with H_2 have energy barriers (Smith et al. 1982; Roberts et al. 2004). In this case, the barriers cannot be overcome unless the gas temperature is >50 K.

Rodgers & Charnley (2002) explain how the relative fractionation of HDCO and D_2CO can provide information about the formation mechanism of the species, and, in particular, whether they have a gas-phase or grain surface origin. They define the quantity F, where:

$$F = \frac{(HDCO/H_2CO)^2}{D_2CO/H_2CO}, \quad (6)$$

and calculate that gas-phase chemistry will produce F values of 1.6 (for the rate coefficients used in our models we calculate 1.3), while surface chemistry models, based on successive reactions of CO with H and D, can give $F \geq 4$ or $F \geq 1$, depending on the exact mechanism.

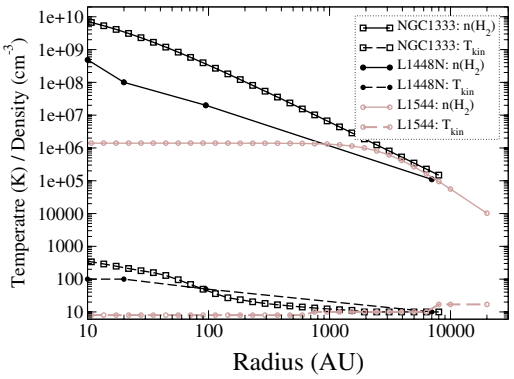

Fig. 7. Observational determinations of the temperature (K) and density (cm^{-3}) as a function of radius towards one prestellar core (L1544) and 2 low-mass protostellar envelopes (NGC 1333 IRAS 4A and L1448N).

For our low-mass sources F ranges from 0.03 to 0.2 (see Table 4). As a comparison, observations of formaldehyde towards the Orion Compact Ridge (OCR; Turner 1990) give F = 6.7, while in IRAS 16293-2422 (Loinard et al. 2000), F = 0.34. Thus, except for the OCR (which is a high-mass source), these results are not consistent with theoretical predictions for gas and grain synthesis, although Rodgers & Charnley also postulate a mechanism whereby grain surface chemistry over a long time period could produce lower F values.

5.1. Low-mass protostellar envelopes

As explained above, the very high N_2D^+/N_2H^+ ratios we observed suggest that our observations are of the cold, depleted envelopes surrounding the protostars, rather than any "hot corino" where large amounts of species have evaporated from grains. The 80″ beam of the ARO 12 m telescope equates to a diameter of 10 000 AU at 140 pc (Taurus) and 15 000 AU at 220 pc (Perseus). Figure 7 shows the temperature and density distribution as a function of radius in a typical prestellar core (L1544; data from Tafalla et al. 2002) together with two of the low-mass protostellar sources in our survey: NGC 1333 (H. Nomura, private communication) and L1448N (from Maret et al. 2004). The cold (<30 K) envelopes of NGC 1333 and L1448N extend from a few hundred to 10 000 AU where they are assumed to merge into the surrounding molecular cloud.

Initially, we have constructed a static protostellar core-envelope model, based on the structure of NGC 1333, shown in Fig. 7. The initial composition of the gas comes from running a series of 42 "prestellar core" models which include reactions of species in the gas-phase and freeze-out of molecules onto grains. Each of these models represents a shell of gas, spaced at equal logarithmic intervals, using the temperature and density profiles of L1544 (see Fig. 7). A comparison of results from this prestellar core model with observations of L1544 has been presented

Table 8. Binding energies for selected surface species. The rate for thermal desorption at a given temperature, $T_{\rm kin}$, is $\sim 10^{12} \exp(-E_{\rm ads}/T_{\rm kin})$ s^{-1}. For N_2, $E_{\rm ads}$ = 380 K generally gives better agreement with observations; the effect of using $E_{\rm ads}$ = 860 K is discussed in Sect. 5.1.1.

Molecule	$E_{\rm ads}$ (K)	Molecule	$E_{\rm ads}$ (K)
N_2	380[a]/860[b]	CH_3OH	2100[c]
CO	930[b]	NH_3	3100[b]
H_2S	1800[c]	CN	1500[c]
H_2CO	1800[c]	H_2O	4800[b]

Note: [a]Bergin & Langer (1997); [b]Sandford & Allamandola (1988); [c]Hasegawa & Herbst (1993).

in Roberts & Millar (2006). The chemistry is evolved for 10^5 yr and then the output molecular abundances from each shell are used as inputs to a similar model which uses the temperature and density profiles determined from observations of NGC 1333. Obviously, this neglects the infall of material through the core, but assuming an infall velocity of 0.1 km s^{-1}, a parcel of gas would move only ~2000 AU in 10^5 yr. In the outer envelope this corresponds to a density increase of a factor $\lesssim$2, which we would not expect to significantly affect the chemistry.

Each model considers 349 gas-phase species, 185 of which contain one or more deuterium atoms. There are ~10 000 gas-phase reactions and ~700 reactions of positive ions with negatively charged grains which result in dissociative recombination. Additionally, the neutral species can accrete onto and desorb from the grain surfaces. We assume a negatively charged grain population with a constant radius (0.1 μm). We assume that the cosmic-ray ionisation rate is the same everywhere and has the standard dark-cloud value: 1.3×10^{-17} s^{-1}.

The only mechanism we include to return material to the gas from the grains is thermal desorption. Each molecule is assigned a binding energy which is used to calculate a rate coefficient for desorption. Binding energies for selected species are listed in Table 8, most of these have been estimated based on experimental work with pure ices, rather than realistic interstellar grain analogues. The unknown desorption energies for many species, and the difficulties in incorporating realistic desorption mechanisms into large models in a systematic way, are major sources of uncertainty. At 10 K the thermal desorption rate for CO is $\sim 10^{-30}$ s^{-1}, so slow as to be effectively zero, but once the temperature reaches 30 K the rate has increased to 10^{-2} s^{-1}. This is orders of magnitude higher than the typical CO accretion rate, so all of the solid CO will evaporate almost instantaneously. Water ice has a much higher binding energy (see Table 8), meaning that the rate for thermal desorption is negligible even at 50 K. At 100 K the rate for thermal desorption of H_2O is $\sim 10^{-9}$ s^{-1} which is comparable with its accretion rate. We have assumed that the binding energy for N_2 is significantly lower than that of CO so that at 10 K the rate for N_2 desorption is $\sim 10^{-5}$ s^{-1}. The N_2 which freezes out is, therefore, rapidly returned to the gas-phase and reacts with molecular hydrogen and deuterium, with their protonated ions (which also have low binding energies due to their low mass), and with cosmic rays and electrons to form e.g. N_2H^+, N_2D^+, and ammonia. The assumption of a relatively low binding energy for N_2 allows us to reproduce the observed distribution of molecules towards prestellar cores, where NH_3 and N_2H^+ do not have the same (or have much smaller) central "holes" due to depletion onto grains, seen for abundant molecules such as CO and CS (Caselli et al. 1999; Tafalla et al. 2002; Bergin et al. 2001, see also Fig. 8). As discussed in Sect. 1,

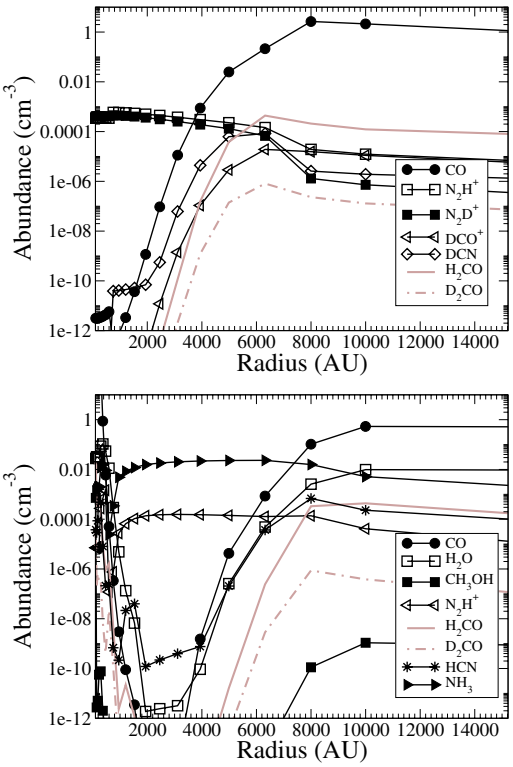

Fig. 8. Predicted abundances of selected molecules as a function of distance from the protostar from the protostellar envelope model. *Top*: at the end of the prestellar core phase; *Bottom*: 10^5 yr after the formation of the protostar.

however, the most recent experiments determined that solid-state processes for CO and N_2 are very similar, under astrophysically relevant conditions (Öberg et al. 2005; Bisschop et al. 2006). Results from chemical models using similar desorption energies for CO and N_2 are presented and discussed in Sect. 5.1.1, below.

We have not explicitly included chemical reactions on the grain surfaces once material freezes out, but, as discussed above, it is likely that the material which desorbs back into the gas will have been altered by chemical processing in the ices. Currently, we simulate the effects of surface hydrogenation in the shells where the bulk of the CO has frozen-out by converting a proportion of the CO ice to H_2CO and CH_3OH, S to H_2S, and O to H_2O. Table 9 (based on that in Osamura et al. 2004) shows the quantities of the molecules we have added in this way. The molecular abundances are based on those observed in warm gas towards protostellar sources. Most of the molecular D/H ratios come from theoretical calculations of grain surface chemistry (Stantcheva & Herbst 2003), although we have lowered the abundances of deuterated water based on recent observational results (Parise et al. 2003, 2005; Butner et al. 2007). We note, though, that, for the models presented here, the exact composition of the gas in the central core is relatively unimportant due to its small size compared to the envelope (see below).

Figure 8 shows the initial distribution of species across the core input into the protostellar envelope model at t = 0 yr (i.e. the output from the prestellar core model) and the distribution at $t = 10^5$ yr. The chemical evolution in the outer envelope surrounding the protostar is very much like that in a prestellar core. Gas-phase species continue to accrete onto grains and the "hole" where CO is totally frozen out increases in size from ~2000 to 4000 AU. There is a small "hot core" region within a few

Table 9. Abundances of molecules assumed to be synthesised by surface chemistry between the prestellar and protostellar phases. For the non-deuterated species the abundances are relative to n(H) while for the deuterated species the abundances are relative to the un-deuterated analogue.

Molecule	Abundance	Molecule	[XD]/[XH]
H_2O	1×10^{-6}	HDO	0.03
H_2CO	2×10^{-8}	HDCO	0.28
		D_2CO	0.02
CH_3OH	1×10^{-7}	CH_3OD	0.18
		CH_2DOH	0.64
		CH_2DOD	0.11
		CHD_2OH	0.14
		CHD_2OD	0.03
		CD_3OH	0.012
		CD_3OD	0.0023
H_2S	2×10^{-9}	HDS	0.33
		D_2S	0.03

hundred AU of the protostar where material has evaporated from the grains and a rich gas-phase chemistry is occurring.

Figure 9 shows evolution of the chemistry predicted in different regions of the protostellar envelope. At 10 AU (top panel) the temperature is high enough to evaporate the bulk of the grain mantle almost instantaneously, so CO, H_2O, CH_3OH and H_2S are abundant. The ionisation fraction is very low due to the high density so the N_2H^+ abundance is also low. The high temperature means very little deuterium fractionation for the molecular ions (H_2D^+, N_2D^+, DCO^+, etc.). We have assumed that the amount of H_2CO formed via hydrogenation of CO on the grain surface is two and a half times the amount which formed in the gas-phase and then accreted, so the formaldehyde fractionation in the post-evaporation gas is set by the surface chemistry.

At 100 AU (second panel of Fig. 9) the temperature is ∼40 K so CO still rapidly desorbs from the grains. Water, formaldehyde, and methanol are more tightly bound, though, (see Table 8) so only a small fraction of these molecules desorb. After the temperature is raised, H_2D^+ is rapidly destroyed by H_2 and its fractionation falls. It then takes only 10−20 yr for the DCO^+/HCO^+ and N_2D^+/N_2H^+ ratios to follow.

At 4000 AU (third panel of Fig. 9) the physical conditions are similar to those at the centre of a prestellar core. Carbon monoxide was already heavily depleted at the beginning of the protostellar phase and so the molecular D/H ratios are very high in this region, although the abundances of all but the nitrogen-bearing species are relatively low.

In the outer envelope at 10 000 AU (bottom panel of Fig. 9) the physical conditions are more like those found in a dark molecular cloud. Molecular D/H ratios increase as species accrete onto grains until, after a further $\sim 10^6$ yr, all the heavier species have frozen out.

Figure 10 shows cumulative column densities for selected molecules predicted by the model, at different times, moving from the outer to the inner region of the low-mass protostellar envelope. For the C- and O- bearing species, the inner envelope region between a few hundred and a few thousand AU doesn't contribute to the column density, as these species are mostly frozen onto the grains. The decrease in CO in the outer envelope over time, due to freeze-out, is apparent. The CO abundance increases by 2−4 orders of magnitude at radii <200 AU, but this is much smaller than the 20 000 AU total radius. There is a large jump in formaldehyde abundance at 100 AU at early times due to evaporation from grains. After $\sim 10^4$ yr, though, a significant proportion of the formaldehyde has been destroyed (see second panel of Fig. 9). For N_2D^+ there is no central enhancement in the column density, as the ionisation fraction is very low at high densities, but the inner envelope region between 1000 and 10 000 AU does contribute to the column density until $\sim 10^6$ yr, when even the N-bearing species have frozen onto the grains.

In order to compare directly with the observations we have calculated beam-averaged column densities from the protostellar envelope model. Results for selected species as a function of time are shown in Fig. 11. These assume an 80″ FWHM beam and a source distance of 220 pc (appropriate for NGC 1333). The first thing that is apparent is that the predicted D_2CO/H_2CO ratio is more than 10 times less than we observed. The column densities are largely determined by the material in the outer envelope (where the abundance of D_2CO is 3 orders of magnitude less than H_2CO; see Fig. 8), since even though the the density of the "hot-core" region is ∼3 orders of magnitude higher than that of the outer envelope, the envelope is so much larger than the core that it contains 10^4 times the mass. The D_2CO/H_2CO ratio does reach 0.01 at ∼4000 AU (see Fig. 9), but the abundance of formaldehyde is this region is several orders of magnitude lower than at 10 000 AU.

We observed D_2CO column densities of $\sim 10^{12}$ cm^{-2}, whereas the model predicts $N(D_2CO) < 10^{11}$ cm^{-2}. For HDCO, however, the agreement is much better: most of the observed column densities were a few $\times 10^{12}$ and the $HDCO/H_2CO$ ratios were 0.02−0.07. At 10^5 yr the model predicts N(HDCO) = 2×10^{12} cm^{-2} and $HDCO/H_2CO = 0.06$.

This model predicts very high N_2D^+ fractionation, since nitrogen bearing species remain relatively abundant closer to the protostar at 2000−4000 AU. After 10^5 yr the predicted N_2D^+/N_2H^+ ratio is 0.3 and the column density of N_2D^+ is $\sim 3 \times 10^{12}$ cm^{-2}. This fractionation is consistent with the highest ratios measured by our survey and the observed column densities towards these sources are within a factor of 2 of the model prediction.

In Paper I we observed HCN and DCN towards most of the same low-mass protostellar sources, finding DCN/HCN ratios of 0.03−0.06 and DCN column densities of $1-4 \times 10^{12}$ cm^{-2}. The model prediction of $N(DCN) = 2 \times 10^{12}$ cm^{-2} agrees very well with these observations, although the predicted DCN/HCN ratio of 0.09 is slightly too high.

One major uncertainty in the deuterium chemistry models is the rate for the reaction of H_3^+ with HD, which is a key reaction for deuterium fractionation at low temperatures. Experiments at 10 K (Gerlich et al. 2002) have suggested that this reaction might proceed ∼5 times slower than the Langevin rate normally assumed (Millar et al. 1989; Giles et al. 1992). A detailed consideration of the effects of slowing the fractionation reactions on one-point chemical models has been presented by Roberts et al. (2002b). The deuterium fractionation at low temperatures also depends on the ortho:para ratios of the reacting species, particularly H_2, which are not well known (Walmsley et al. 2004; Flower et al. 2006). For the models presented in this section, which involve averaging over regions with different physical conditions, using slower rates for the fractionation reactions does not have a drastic effect. The predicted column density ratios are reduced by factors of 2−4, but (again with the exception of D_2CO) this is not inconsistent with observations towards many of our sources.

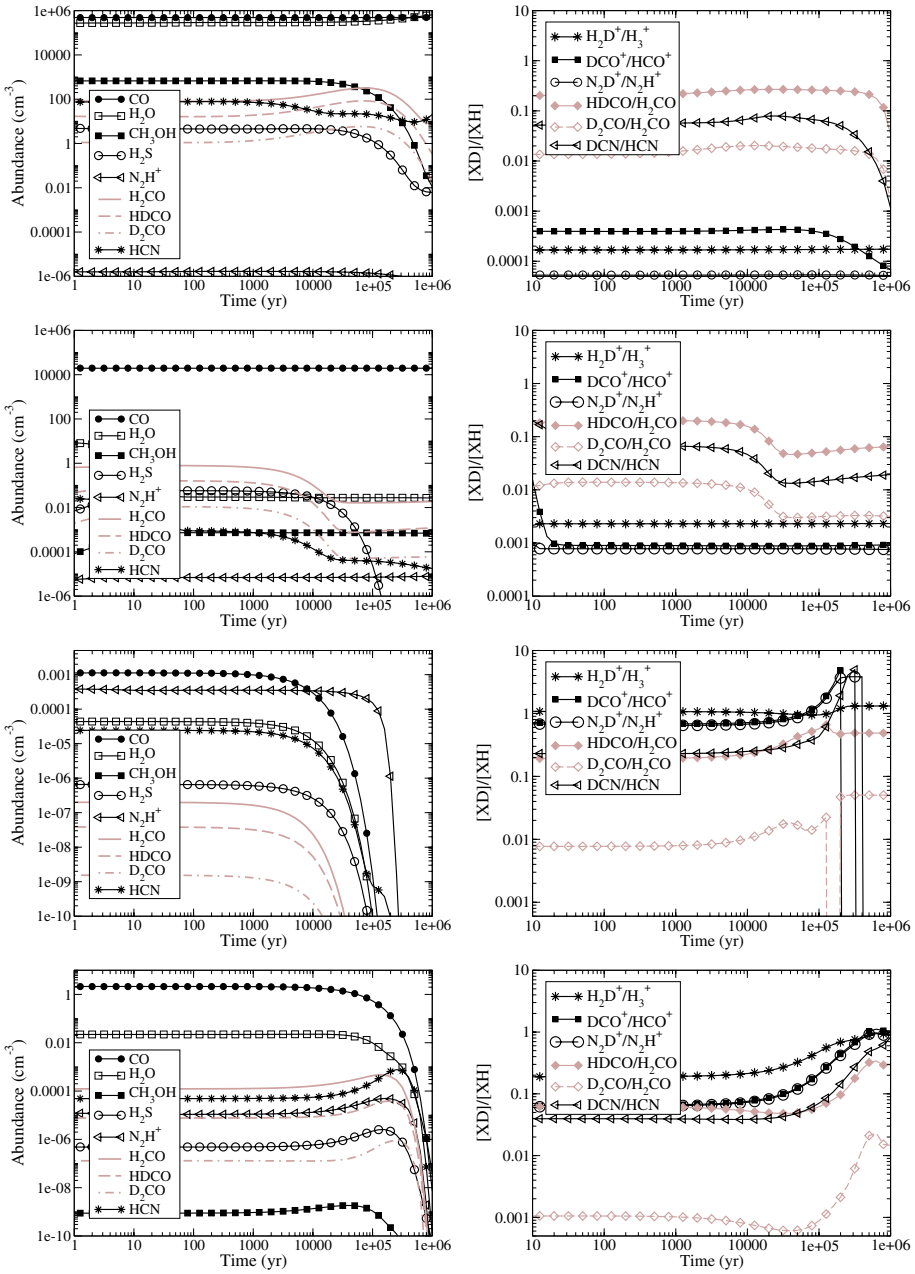

Fig. 9. The predicted evolution of molecular abundances (*left panel*) and D/H ratios (*right panel*) after the formation of the central protostar in selected regions of the protostellar envelope. *From top to bottom*: 10 AU, $T_{\rm kin}$ = 340 K, $n(H_2) = 3 \times 10^9$; 100 AU, 40 K, 10^8 cm^{-3}; 4000 AU, 10 K, 3×10^5 cm^{-3}; 10 000 AU, 10 K, 3×10^4 cm^{-3}.

5.1.1. The binding energy for N_2 and a comparison of N_2D^+ and DCO^+ fractionation

We have also run the models using an N_2 binding energy of 860 K, which is consistent with the experimental result: $E_{\rm ads}(N_2) = 0.923\,E_{\rm ads}$(CO) (Öberg et al. 2005). Results are shown in Figs. 12 and 13. The nitrogen bearing species now freeze out on a similar timescale to other molecules so at the start of the protostellar phase (top panel of Fig. 12) there is a hole of radius ∼2000 AU at the centre where no heavy species remain in the gas-phase. This hole increases in diameter as the envelope surrounding the protostar evolves and a hot core region forms close to the protostar (bottom panel of Fig. 12). Except for the distribution of the N-bearing species, the overall picture is very similar to the previous model.

Adopting a higher binding energy for N_2 does cause the column density of D_2CO and the average D_2CO/H_2CO ratio to increase, but they are still significantly lower than the observations (see Fig. 13). In fact, many of the molecular D/H ratios have increased (although the N_2D^+/N_2H^+ ratio is lower) since there is a strong anti-correlation between the abundance of heavy species in the gas-phase (including N_2 and NH_3) and the level of deuterium fractionation (see e.g. Roberts et al. 2004). The beam-averaged column density of N_2D^+ has fallen from a few $\times 10^{12}$ cm^{-2} at times $<10^5$ yr to $\lesssim 3 \times 10^{11}$ cm^{-2}. This is more than 10 times lower than the observation towards NGC 1333 IRAS 4A, but is similar to those towards L1527, B5IRS1, RNO43, and HH111. L1527 is the only one of these sources in which we also observed N_2H^+, giving N_2D^+/N_2H^+ = 0.05. This observed ratio is lower than those predicted by either protostellar envelope model.

In Fig. 14 we compare N_2D^+/N_2H^+ and DCO^+/HCO^+ ratios observed towards six different sources: dark clouds/starless cores (TMC-1, TMC-2, L1400G), prestellar cores (L1544 and L134N) and a protostellar envelope (L1551 IRS5). In all these sources the N_2D^+ fractionation is 2 to 100 times higher than the DCO^+ fractionation (there is one exception to this, not plotted in

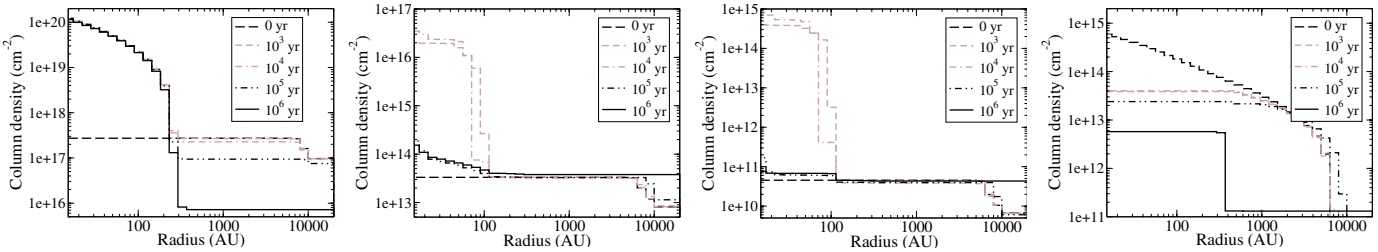

Fig. 10. Cumulative column densities from the model at different times for (*from left to right*): CO, H_2CO, D_2CO, N_2D^+. The extreme right-hand side of each plot shows the column density through only the outermost layer of the cloud; as the radius decreases, column densities through successive inner layers are added. Note: these only illustrate the relative contribution from different layers at different times, and do not represent what one would expect to observe by pointing a telescope away from the source centre.

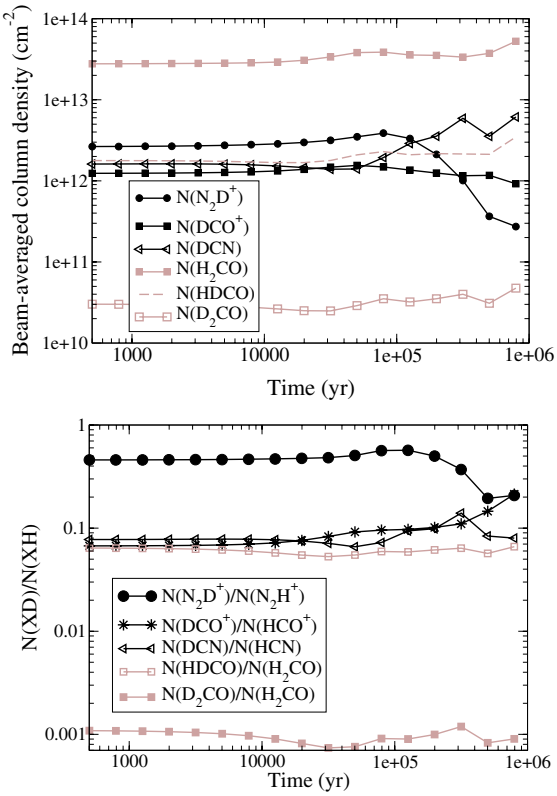

Fig. 11. *Top*: predicted molecular column densities evolving over time from the protostellar envelope model that we would expect to observe for a source at distance of 220 pc with an 80″ telescope beam. *Bottom*: average molecular D/H ratios from the same model.

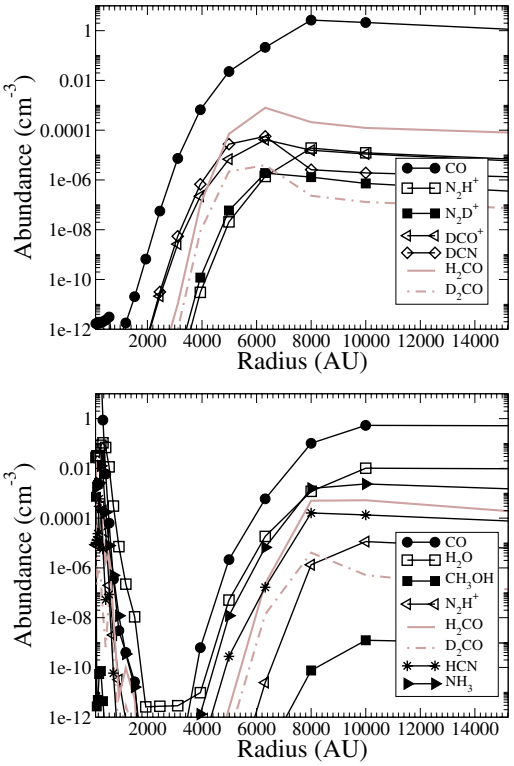

Fig. 12. As for Fig. 8, except that we assume CO and N_2 have similar binding energies.

Fig. 14: Butner et al. (1995) measured $DCO^+/HCO^+ = 0.035$ towards L1498, but we did not detect N_2D^+, using the same 12 m telescope, in this source and calculate $N_2D^+/N_2H^+ < 0.014$). For a given set of physical conditions, models of deuterium chemistry predict that, even if HCO^+ and N_2H^+ have different abundances, DCO^+ and N_2D^+ will have the same fractionation (see Fig. 9), since they form directly from deuterated H_3^+. The model presented in Sect. 5.1 predicts that the observed (i.e. based on beam-averaged column densities) N_2D^+ fractionation will be 5−6 times higher than the DCO^+ fractionation. Since N_2 resists freeze-out, N_2H^+ and N_2D^+ remain abundant in the inner envelope (∼4000 AU), where fractionation is very high, for much longer than HCO^+ and DCO^+. The overall DCO^+ fractionation, therefore, reflects that in the outer envelope, whereas emission from both the inner and outer envelope contributes to the N_2D^+ fractionation.

If we assume, though, that the N_2 which collides with the grains remains frozen (as in the model presented in this section) then the distribution of N-bearing species across the core is very similar to the C- and O- bearing species and we predict $N_2D^+/N_2H^+ \lesssim 1.5$ times higher than DCO^+/HCO^+. Incorporating the most recent experimental results for the binding energies of N_2 and CO on interstellar-analogue surfaces, therefore, gives us significantly worse agreement with observational results. Other authors (Aikawa et al. 2001; Vastel et al. 2006) have found that the difference in N_2D^+ and DCO^+ fractionation can be explained by the fact that CO is a major destroyer of N_2H^+ and N_2D^+ in the gas-phase, so the loss of CO onto grains causes an enhancement in their abundances. In our models, the major loss mechanism for N_2H^+ is collision with negatively charged grains (we assume that this produces N_2

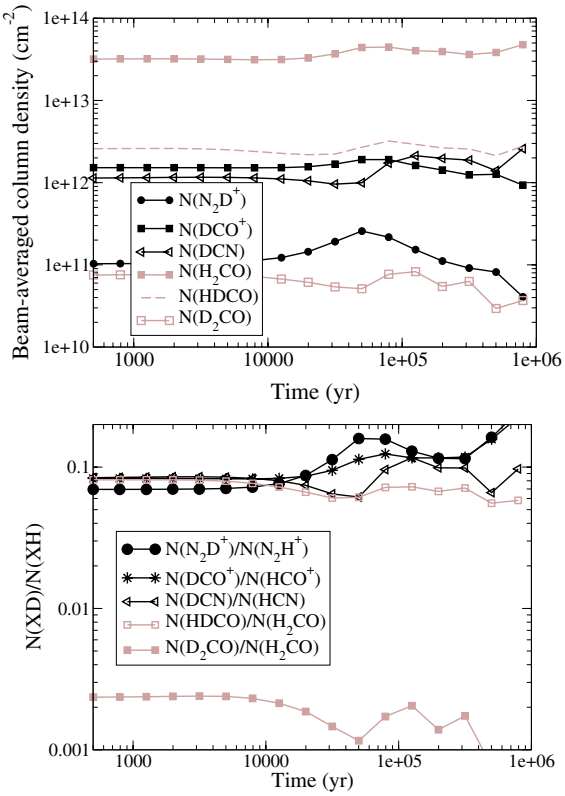

Fig. 13. As for Fig. 11, except that we assume CO and N_2 have similar binding energies.

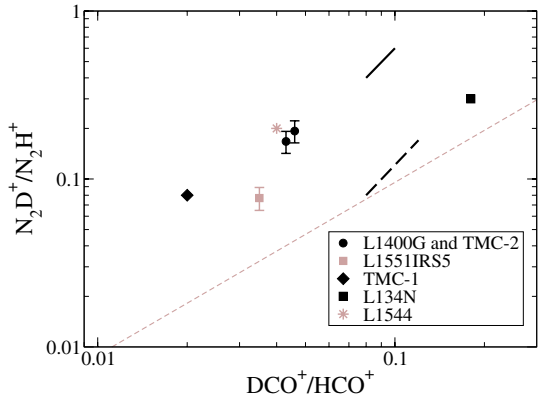

Fig. 14. A comparison of the N_2D^+ and DCO^+ fractionation observed towards a selection of sources compiled from our observations and results from the literature: Butner et al. (1995), Caselli et al. (2002b), Gerin et al. (2001), Tiné et al. (2000), Williams et al. (1998). The grey dashed line shows $x = y$; the solid black line indicates the range of values predicted by a chemical model of a low-mass protostellar envelope which assumes N_2 can desorb efficiently from grain surfaces at lower temperatures than CO, while the dashed black line shows the prediction from the same model when N_2 and CO are assumed to evaporate at the same rate.

and H, which are returned to the gas-phase; see Roberts et al. 2004), so the depletion of CO does not have a significant effect.

5.2. Hot molecular cores

The molecular D/H ratios previously determined towards our sample of HMCs are: HDO/$H_2O \sim 10^{-4}$ (Gensheimer et al. 1996), DCN/HCN $\sim 10^{-3}$ (Hatchell et al. 1998a),

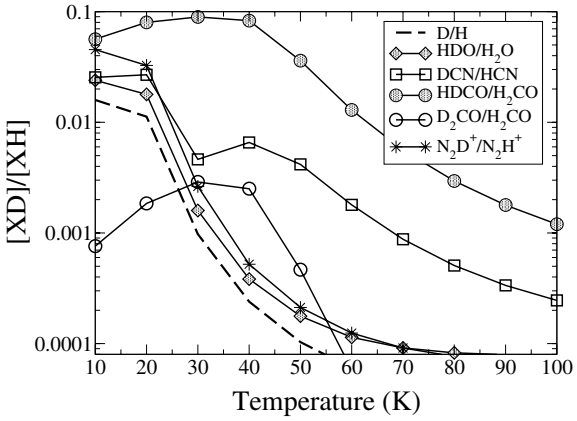

Fig. 15. Steady-state molecular D/H ratios as a function of temperature from gas-phase chemical models using $n(H_2) = 10^6$ cm^{-3}, a cosmic ray ionisation rate of 1.3×10^{-17} s^{-1} and a visual extinction of 10 mag.

and HDS/$H_2S < 10^{-3}$ (Hatchell et al. 1999). The water observations were carried out using the IRAM 30 m telescope (11−12″ beam), while the other observations were made with the JCMT (∼20″ beam). Figure 15 shows the equilibrium (steady-state) fractionation predicted by gas-phase ion-molecule chemistry for HDO, DCN, HDCO, D_2CO and N_2D^+ for temperatures varying between 10 and 100 K. The H_2 density was assumed to be 10^6 cm^{-3}, but the curves for $n(H_2) = 10^4$ cm^{-3} are very similar. Before the onset of star-formation molecules accrete onto grain surfaces and the level of deuteration is "frozen in" until the star forms and heats the gas, returning the molecules to the gas-phase. Molecular D/H ratios observed towards HMCs can, therefore, be significantly higher than the equilibrium values at 100−200 K. The exceptions to this are molecular ions, such as N_2D^+ and N_2H^+, which are expected to dissociate when they strike a negatively charged grain, so the D/H ratios for molecular ions set in the gas-phase are not preserved in the ice mantles. Once the gas is heated the N_2D^+/N_2H^+ ratio resets to its equilibrium value much more rapidly than the neutral species (see also the top two panels of Fig. 9). The upper limits on the N_2D^+/N_2H^+ ratios towards the HMCs suggest that the bulk of the gas is warmer than 30 K. Thus, even if the HMCs are much smaller than the telescope beam (a core with diameter 0.1 pc at a distance of 4 kpc subtends an angle of only 5″), they are not surrounded by a very cold envelope like the low-mass protostars.

Comparing the other curves in Fig. 15 with the ratios observed towards HMCs assumes that the fractionation was set in the gas-phase before the onset of star-formation, that there was not a long period of freeze-out onto grains at low temperatures, and that the grains merely acted as a repository for the molecules which accreted. The curve for HDS fractionation would closely follow that of HDO, but the actual abundance of HDS and H_2S formed in the gas phase at these temperatures is very low, so it is unlikely that the hydrogen sulphide observed towards HMCs could have been synthesised in the gas-phase. Instead, we have plotted the atomic D/H ratio and, if simple hydrogenation schemes for surface chemistry (e.g. Brown & Millar 1989; Turner 1990; Stantcheva & Herbst 2003) are a good approximation to reality, we expect the relative abundance of HDS to H_2S formed on the surface to be similar to the relative amount of D to H accreting onto the surface.

Of course, if hydrogen sulphide is forming on grain surfaces, then, clearly, we must allow the possibility that other molecules may be. Observations show that the bulk of the grain mantles

consists of water ice (see e.g. Whittet et al. 1996; Keane et al. 2001; Gibb et al. 2004, and references therein) so H_2O must form efficiently. Experiments suggest that the CO which freezes out can be converted to formaldehyde and methanol (Watanabe & Kouchi 2002; Watanabe et al. 2003, 2004). Figure 15 shows that we would expect the HDO forming on the grain surface (from atomic D) to have a similar fractionation to that formed in the gas-phase, but illustrates the point made by Turner (1990) and Rodgers & Charnley (2002) that surface chemistry could dramatically alter the $HDCO/H_2CO$ and D_2CO/H_2CO ratios.

Assuming that H_2S is formed by surface chemistry, the upper limits on the HDS/H_2S ratios in the HMCs constrain the ice formation temperature to >30 K, while the observed HDO/H_2O ratios suggest temperatures of 50−60 K. The DCN/HCN ratios are reproduced at $T \sim 60-70$ K, but it is possible that DCN fractionation is lowered in the gas-phase post-evaporation (Hatchell et al. 1998a), so these temperatures are upper limits.

The formaldehyde fractionation remains relatively high until the temperature reaches ∼60 K, due to the fact that the deuterated CH_3^+ ions have a higher energy barrier to destruction by H_2 than the deuterated H_3^+ ions (see Sect. 5). The $HDCO/H_2CO$ ratios of 0.01 and 0.03, along with D_2CO/H_2CO upper limits of 0.001 measured towards G34.26 and G75.78 are also consistent with formation temperatures of 50−60 K, if the bulk of the formaldehyde was formed in the gas-phase. Towards G31.41, however, the $HDCO/H_2CO$ ratio was only 0.002, which would imply gas-phase temperatures >90 K. This is inconsistent with the fractionation of DCN and HDO, so it seems likely that in this source the $HDCO/H_2CO$ ratio set in the gas-phase was then diluted by the formation of additional formaldehyde on the grains. Assuming that both gas-phase and grain surface formation are, therefore, also important in G34.26 and G75.78, all we can say is that the gas-temperature was <60 K.

These molecular D/H ratios are all consistent with the HMCs having formed out of relatively warm (50 K) gas. They suggest that surface chemistry has affected the composition of the gas, but that there was not a long period of accretion at very low temperatures, such as is implied by the results for the low-mass protostars.

6. Discussion

We have measured DCN/HCN, $HDCO/H_2CO$, D_2CO/H_2CO and N_2D^+/N_2H^+ ratios towards a number of low-mass protostellar sources at different evolutionary stages and in different molecular clouds. The N_2D^+/N_2H^+ ratios are all >0.01 which implies that the bulk of the emission comes from a region where the gas temperature is <25 K; i.e. from the extended envelope surrounding the protostars. In four of the sources the N_2D^+ fractionation was >0.1, suggesting that the surrounding envelopes are depleted in CO. A static protostellar core-envelope model can explain the deuterium fractionation in most of these molecules, but the D_2CO/H_2CO ratio remains a problem. The physical model we have adopted is relatively simple, but this does not appear to be the main problem, since the average ratios from the model are close to those predicted by theory and the theory does not reproduce the relative abundances of HDCO and D_2CO which are observed. It seems more likely that there is a chemical process missing from both the theory and models. A candidate for this is formation of D_2CO on grain surfaces, followed by a non-thermal desorption mechanism which is efficient even at 10 K, *but* if this mechanism also returns CO to the gas-phase, it will act to suppress the deuterium fractionation in molecular ions like N_2D^+ and DCO^+.

This study finds no compelling evidence for an evolutionary trend where the formaldehyde fractionation increases as the N_2D^+ fractionation decreases, but we plan to measure N_2D^+/N_2H^+ ratios in more of the sources in which we have D_2CO/H_2CO ratios. We are also developing models of collapsing protostellar core-envelope systems (Roberts et al. in preparation) which will explicitly include grain-surface chemistry along with time-dependent heating of the gas and desorption. These should provide better predictions for the evolution of molecular D/H ratios in star-forming regions and may explain why two of the low-mass protostellar envelopes we observed have N_2D^+ fractionation <0.1, which does not require CO to be heavily depleted.

We have also measured N_2D^+/N_2H^+ ratios towards five cold, starless cores. The only systematic difference between these observations and the low-mass protostars is that the lines from the cold cores are narrower. Three of the starless cores have N_2D^+/N_2H^+ ratios >0.1, similar to the ratio observed towards the prestellar core L1544, suggesting that these sources also have significant, extended CO depletion. The ratios of <0.03 towards the other two starless cores are more consistent with a dark cloud gas-phase chemistry (see e.g. Roberts & Millar 2000).

Towards the hot molecular cores, associated with high mass star formation, we have measured $HDCO/H_2CO$ ratios and calculated upper limits on the D_2CO and N_2D^+ fractionation. Comparing these, along with DCN/HCN, HDO/H_2O, and HDS/H_2S ratios determined by other authors, to the predicted equilibrium fractionation as a function of temperature, we find that the observations are all consistent with the molecules having formed when the gas temperature was 50−60 K. The current temperature at the centre of the cores appears to be >80 K and the observations of water and hydrogen sulphide (among others, see Hatchell et al. 1998b) confirm that grain surface chemistry has affected the composition of the gas. Thus, the fractionation of the deuterated molecules that are observed was most likely set during an earlier stage of evolution, before the protostar formed, and preserved in the grain mantles. It does not appear that these cores underwent long periods of accretion at low temperatures, or that they are currently surrounded by cold, depleted envelopes, like the low-mass protostars. This suggests that the star formed out of relatively warm gas and dust (50−60 K), which would support current theories concerning the differences between low and high-mass star formation: high mass stars form more rapidly and in clusters, whereas low mass stars form in isolation after a relatively long prestellar core phase.

The upper limits on the N_2D^+/N_2H^+ ratios suggest that the envelopes surrounding the HMCs have temperatures >30 K. Recently, though, Fontani et al. (2006) detected N_2D^+ in the vicinity of other high-mass protostellar candidates, sources which are probably younger than ours, finding N_2D^+/N_2H^+ ratios of $\sim 10^{-2}$. This indicates the presence of cold (<25 K) gas, but not necessarily heavy molecular depletion (in fact, Fontani et al. measure CO depletion factors of ∼3). They conclude that this cold gas could either be the remnant of a prestellar core phase, or could be located in nearby starless cores.

Clearly, further observations of both low and high-mass protostars at higher spatial resolution are required in order to determine the chemical history of the gas and dust.

Acknowledgements. The 12 m Telescope is a facility of the National Science Foundation currently operated by the University of Arizona Steward Observatory under a loan agreement with the National Radio Astronomy Observatory. The James Clerk Maxwell Telescope is operated by The Joint Astronomy Centre on behalf of the Particle Physics and Astronomy Research Council of the United Kingdom, the Netherlands Organisation for Scientific Research, and the

National Research Council of Canada. The authors would like to thank Albrecht Sievers and Manolo Ruiz at IRAM for carrying out the IRAM 30 m observations. Much of this work was carried out while the authors were employed by the University of Manchester, UK. Astrophysics at Queens University Belfast and The University of Manchester is supported by PPARC.

References

Aikawa, Y., Ohashi, N., Inutsuka, S.-i., Herbst, E., & Takakuwa, S. 2001, ApJ, 552, 639
Bacmann, A., Lefloch, B., Ceccarelli, C., et al. 2002, A&A, 389, L6
Bacmann, A., Lefloch, B., Ceccarelli, C., et al. 2003, ApJ, 585, L55
Bergin, E. A., & Langer, W. D. 1997, ApJ, 486, 316
Bergin, E. A., Ciardi, D. R., Lada, C. J., Alves, J., & Lada, E. A. 2001, ApJ, 557, 209
Bisschop, S. E., Fraser, H. J., Öberg, K. I., van Dishoeck, E. F., & Schlemmer, S. 2006, A&A, 449, 1297
Brown, P. D., & Millar, T. J. 1989, MNRAS, 240, 25P
Butner, H. M., Lada, E. A., & Loren, R. B. 1995, ApJ, 448, 207
Butner, H. M., Charnley, S. B., Ceccarelli, C., et al. 2007, ApJ, 659, L137
Caselli, P., Walmsley, C. M., Tafalla, M., Dore, L., & Myers, P. C. 1999, ApJ, 523, L165
Caselli, P., Walmsley, C. M., Zucconi, A., et al. 2002a, ApJ, 565, 331
Caselli, P., Walmsley, C. M., Zucconi, A., et al. 2002b, ApJ, 565, 344
Ceccarelli, C., Castets, A., Caux, E., et al. 2000a, A&A, 355, 1129
Ceccarelli, C., Loinard, L., Castets, A., Tielens, A. G. G. M., & Caux, E. 2000b, A&A, 357, L9
Ceccarelli, C., Loinard, L., Castets, A., et al. 2001, A&A, 372, 998
Crapsi, A., Caselli, P., Walmsley, C. M., et al. 2005, ApJ, 619, 379
Dickens, J. E., & Irvine, W. M. 1999, ApJ, 518, 733
Dore, L., Caselli, P., Beninati, S., et al. 2004, A&A, 413, 1177
Doty, S. D., van Dishoeck, E. F., & Tan, J. C. 2006, A&A, 454, L5
Flower, D. R., Pineau Des Forêts, G., & Walmsley, C. M. 2006, A&A, 456, 215
Fontani, F., Caselli, P., Crapsi, A., et al. 2006, A&A, 460, 709
Gensheimer, P. D., Mauersberger, R., & Wilson, T. L. 1996, A&A, 314, 281
Gerin, M., Pearson, J. C., Roueff, E., Falgarone, E., & Phillips, T. G. 2001, ApJ, 551, L193
Gerlich, D., Herbst, E., & Roueff, E. 2002, Planet. Space Sci., 50, 1275
Gibb, E. L., Whittet, D. C. B., Boogert, A. C. A., & Tielens, A. G. G. M. 2004, ApJS, 151, 35
Giles, K., Adams, N. G., & Smith, D. 1992, J. Phys. Chem., 96, 7645
Goldsmith, P. F., & Langer, W. D. 1999, ApJ, 517, 209
Hasegawa, T. I., & Herbst, E. 1993, MNRAS, 261, 83
Hatchell, J. 2003, A&A, 403, L25
Hatchell, J., Millar, T. J., & Rodgers, S. D. 1998a, A&A, 332, 695
Hatchell, J., Thompson, M. A., Millar, T. J., & MacDonald, G. H. 1998b, A&AS, 133, 29
Hatchell, J., Roberts, H., & Millar, T. J. 1999, A&A, 346, 227
Kahane, C., Lucas, R., Frerking, M. A., Langer, W. D., & Encrenaz, P. 1984, A&A, 137, 211
Keane, J. V., Tielens, A. G. G. M., Boogert, A. C. A., Schutte, W. A., & Whittet, D. C. B. 2001, A&A, 376, 254
Lis, D. C., Roueff, E., Gerin, M., et al. 2002, ApJ, 571, L55
Loinard, L., Castets, A., Ceccarelli, C., et al. 2000, A&A, 359, 1169
Loinard, L., Castets, A., Ceccarelli, C., Caux, E., & Tielens, A. G. G. M. 2001, ApJ, 552, L163
Loinard, L., Castets, A., Ceccarelli, C., et al. 2002, Planet. Space Sci., 50, 1205
Maret, S., Ceccarelli, C., Caux, E., et al. 2004, A&A, 416, 577
Maret, S., Ceccarelli, C., Tielens, A. G. G. M., et al. 2005, A&A, 442, 527
Millar, T. J., Bennett, A., & Herbst, E. 1989, ApJ, 340, 906
Öberg, K. I., van Broekhuizen, F., Fraser, H. J., et al. 2005, ApJ, 621, L33
Osamura, Y., Roberts, H., & Herbst, E. 2004, A&A, 421, 1101
Osamura, Y., Roberts, H., & Herbst, E. 2005, ApJ, 621, 348
Parise, B., Ceccarelli, C., Tielens, A. G. G. M., et al. 2002, A&A, 393, L49
Parise, B., Simon, T., Caux, E., et al. 2003, A&A, 410, 897
Parise, B., Castets, A., Herbst, E., et al. 2004, A&A, 416, 159
Parise, B., Caux, E., Castets, A., et al. 2005, A&A, 431, 547
Parise, B., Ceccarelli, C., Tielens, A. G. G. M., et al. 2006, A&A, 453, 949
Redman, M. P., Rawlings, J. M. C., Nutter, D. J., Ward-Thompson, D., & Williams, D. A. 2002, MNRAS, 337, L17
Roberts, H., & Millar, T. J. 2000, A&A, 361, 388
Roberts, H., & Millar, T. J. 2006, R. Soc. London Philos. Trans. Ser. A, 364, 3063
Roberts, H., Fuller, G. A., Millar, T. J., Hatchell, J., & Buckle, J. V. 2002a, A&A, 381, 1026
Roberts, H., Herbst, E., & Millar, T. J. 2002b, MNRAS, 336, 283
Roberts, H., Herbst, E., & Millar, T. J. 2004, A&A, 424, 905
Rodgers, S. D., & Millar, T. J. 1996, MNRAS, 280, 1046
Rodgers, S. D., & Charnley, S. B. 2002, Planet. Space Sci., 50, 1125
Saito, S., Ozeki, H., Ohishi, M., & Yamamoto, S. 2000, ApJ, 535, 227
Sandford, S. A., & Allamandola, L. J. 1988, Icarus, 76, 201
Schöier, F. L., Jørgensen, J. K., van Dishoeck, E. F., & Blake, G. A. 2002, A&A, 390, 1001
Smith, D., Adams, N. G., & Alge, E. 1982, J. Chem. Phys., 77, 1261
Stantcheva, T., & Herbst, E. 2003, MNRAS, 340, 983
Tafalla, M., Myers, P. C., Caselli, P., Walmsley, C. M., & Comito, C. 2002, ApJ, 569, 815
Tiné, S., Roueff, E., Falgarone, E., Gerin, M., & Pineau des Forêts, G. 2000, A&A, 356, 1039
Turner, B. E. 1990, ApJ, 362, L29
van der Tak, F. F. S., Schilke, P., Müller, H. S. P., et al. 2002, A&A, 388, L53
Vastel, C., Caselli, P., Ceccarelli, C., et al. 2006, ApJ, 645, 1198
Vastel, C., Phillips, T. G., Ceccarelli, C., & Pearson, J. 2003, ApJ, 593, L97
Walmsley, C. M., Flower, D. R., & Pineau des Forêts, G. 2004, A&A, 418, 1035
Watanabe, N., & Kouchi, A. 2002, ApJ, 571, L173
Watanabe, N., Shiraki, T., & Kouchi, A. 2003, ApJ, 588, L121
Watanabe, N., Nagaoka, A., Shiraki, T., & Kouchi, A. 2004, ApJ, 616, 638
Whittet, D. C. B., Schutte, W. A., Tielens, A. G. G. M., et al. 1996, A&A, 315, L357
Williams, J. P., Bergin, E. A., Caselli, P., Myers, P. C., & Plume, R. 1998, ApJ, 503, 689
Womack, M., Ziurys, L. M., & Wyckoff, S. 1992, ApJ, 387, 417

Online Material

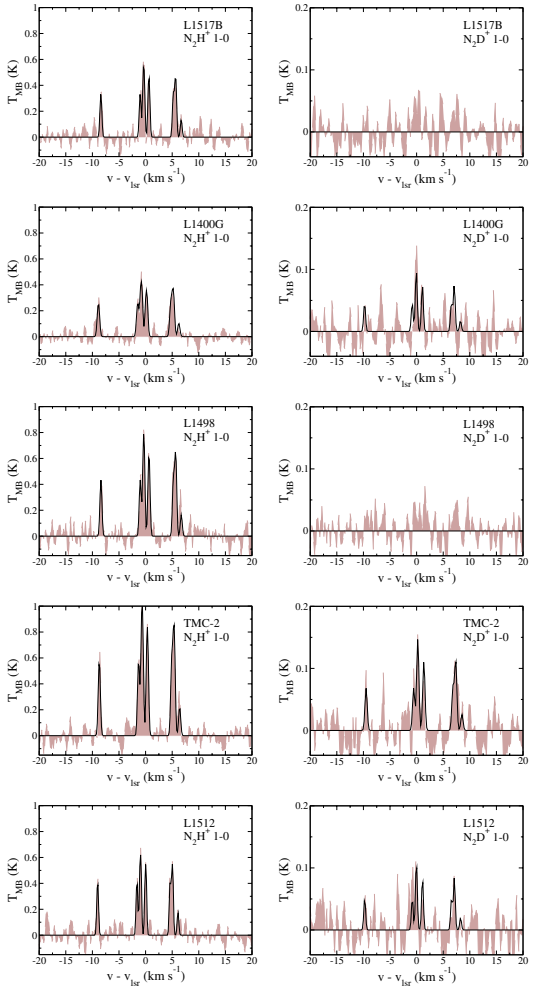

Fig. 1. Spectra of the 1–0 transitions of N_2H^+ (*left panel*) and N_2D^+ (*right panel*) towards cold, starless cores from the UofA 12 m telescope.

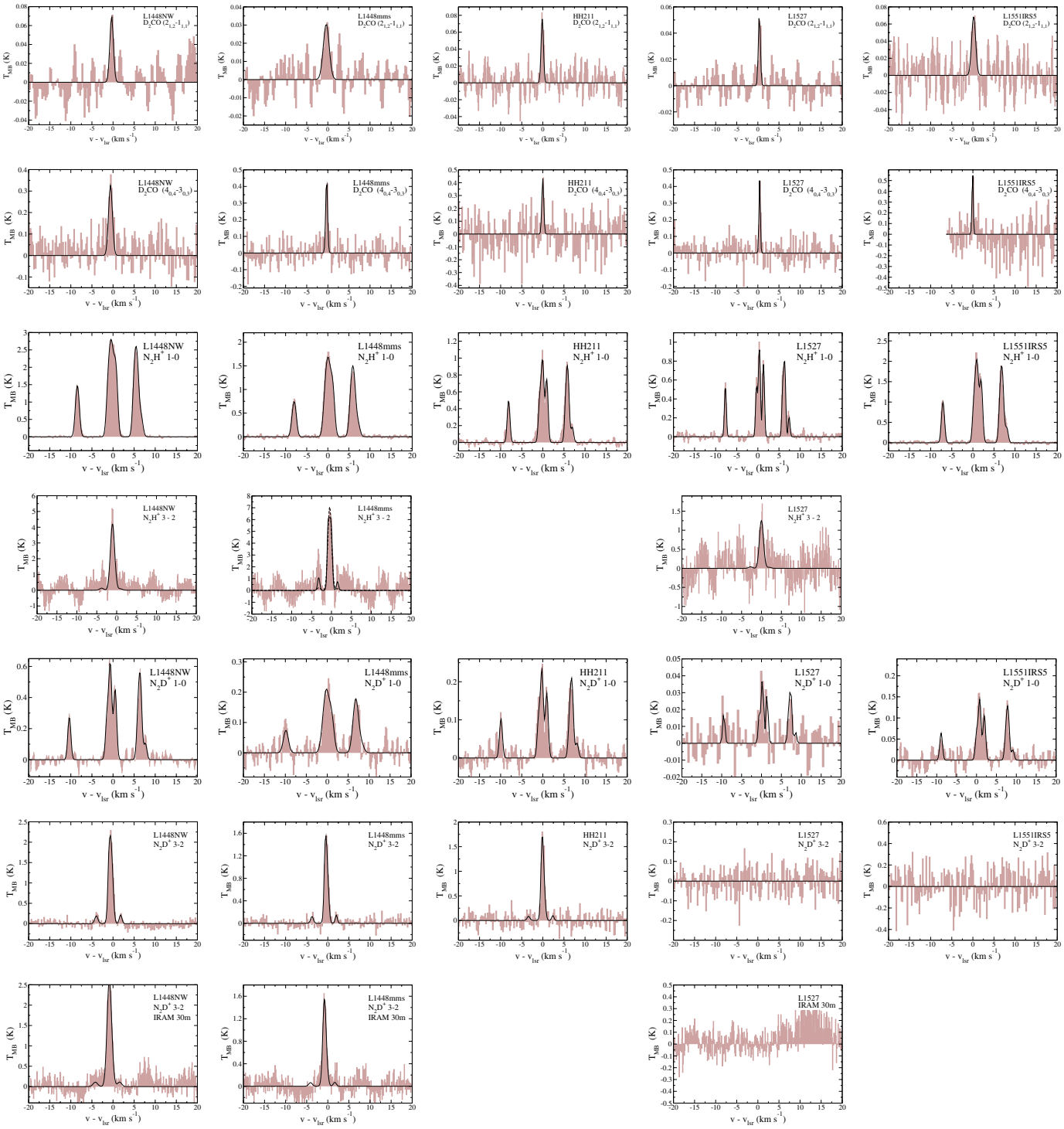

Fig. 2. Spectra observed towards 5 of the low-mass protostellar sources. ROW 1: D_2CO $2_{1,2}-1_{1,1}$ from the UofA 12 m telescopes; ROW 2: D_2CO $4_{0,4}-3_{0,3}$ from the JCMT; ROW 3: N_2H^+ 1–0 multiplets from the UofA 12 m telescope; ROW 4: N_2H^+ 3–2 multiplets observed with the IRAM 30 m telescope (the uncertainty in the CLASS fits for these spectra is illustrated for N_2H^+ in L1448mms: the solid black line shows a fit with $\tau = 8$, while the dashed line shows an alternate fit with $\tau = 0.1$); ROW 5: N_2D^+ 1–0 multiplets from the UofA 12 m telescopes; ROW 6: N_2D^+ 3−2 multiplets from the JCMT; ROW 7: N_2D^+ 3−2 multiplets from the IRAM 30 m telescope.

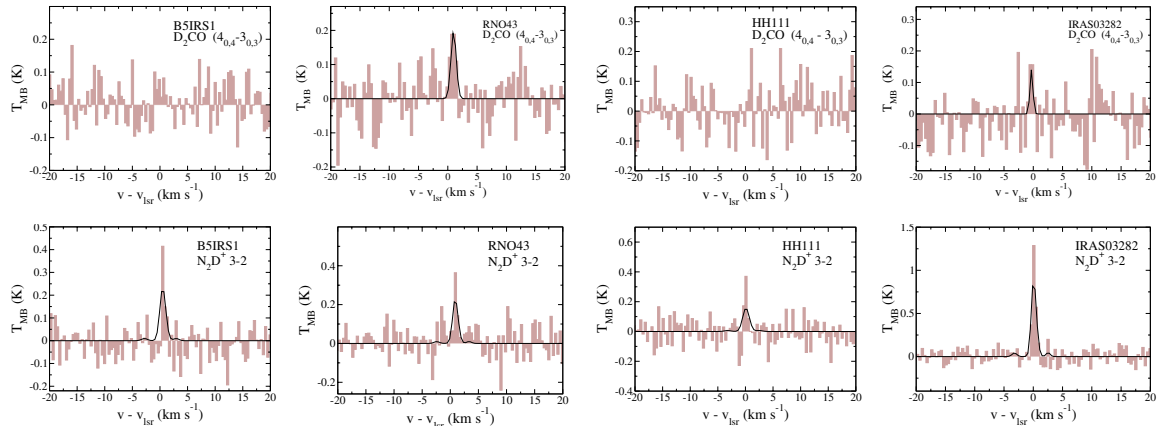

Fig. 3. Spectra observed towards a further 4 low-mass protostellar sources using the JCMT. UPPER ROW: D_2CO $4_{0,4}$–$3_{0,3}$ line; LOWER ROW: N_2D^+ 3–2 multiplet.

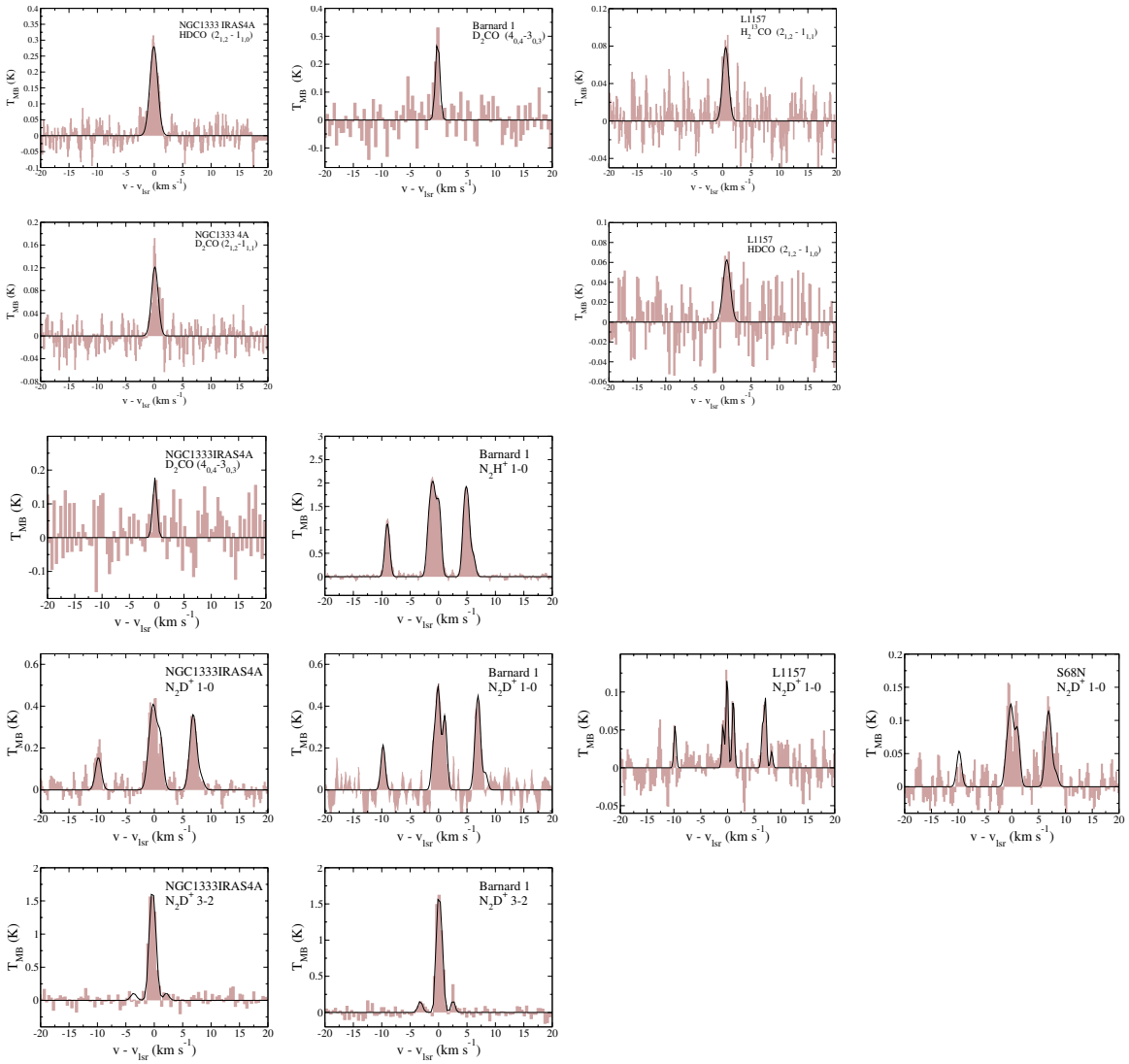

Fig. 4. Spectra observed towards an extra 4 low-mass protostellar sources using the UofA 12 m telescope and the JCMT; lines as described in the top right-hand corner of each spectrum.

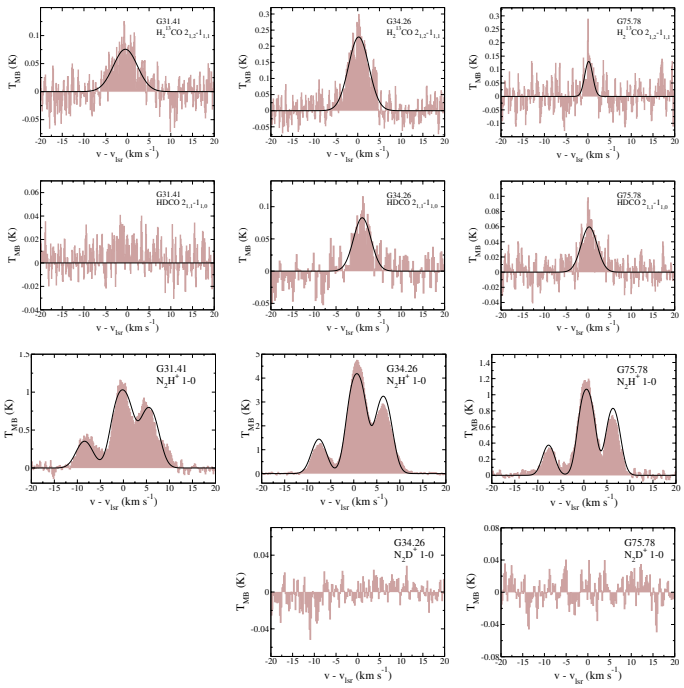

Fig. 5. Spectra observed towards the HMCs using the UofA 12 m telescope. ROW 1: $H_2^{13}CO\ 2_{1,2}-1_{1,1}$ line; ROW 2: HDCO $2_{1,1}-1_{1,0}$ line; ROW 3: N_2H^+ 1–0 multiplet; ROW 4: searches for the N_2D^+ 1−0 multiplet.